

Supporting Information

Thermostability and Photoluminescence under the Magnetic Field of Dy(III) Single-Molecule Magnets

Ye Bi^a, Cheng Chen^b, Yi-Fang Zhao^a, Yi-Quan Zhang^c, Shang-Da Jiang^a,Bing-Wu Wang^{a,*}, Jun-Bo Han^b, Jun-Liang Sun^a, Zu-Qiang Bian^a, Zhe-Ming Wang^a,Song Gao ^{a,*}

Table of Contents

Fig. S1–S4 The molecular structure of compounds 1–4	S4–S5
Fig. S5–S8 The crystal packing of compounds 1–4	S6–S7
Fig. S9–S10 The molecular structure and the crystal packing of compounds 8	S8
Fig. S11–S12 The experimental PXRD patterns and Le Bail fitting for compounds 5–8	S9–S11
Fig. S13 The thermogravity analyses for compounds 1–3 and compound 5–7	S12
Fig. S14 The plots of $1/\chi_M$ vs. T fitted by Curie-Weiss formula for compounds 1–8 and $\chi_M T$ values from experiment and CASSCF calculation for compounds 1–4 and 8	S13
Fig. S15 The M vs. H at 2 K for compounds 1–8 and the CASSCF calculation for compounds 1–4 and 8	S14
Fig. S16–S17 M vs. H/T^1 for compounds 1–8	S15
Fig. S18–S19 The magnetic hysteresis loops for compounds 1–4 and 6–8	S16
Fig. S20–S21 The ac magnetic susceptibilities versus T for compounds 1–8	S17
Fig. S22–S23 The ac magnetic susceptibilities versus v for compounds 1–8 and the Arrhenius fit for 1 and 5	S18
Fig. S24–S25 The optimition of the external magnetic field for compounds 1–4 and 6–8 and the Arrhenius fit for 2–3 and 6–7	S19
Fig. S26–S27 The ac magnetic susceptibilities versus T under 1000 Oe for compounds 1–8	S20
Fig. S28–S29 The ac magnetic susceptibilities versus v under 1000 Oe for compounds 1–8	S21
Fig. S30–S31 Cole-Cole fitting under 0 and 1000 Oe dc field for compounds 1–8	S22
Fig. S32 The excited spectrum of 4 and emission spectra of compounds 1–4 and 8	S23
Fig. S33 The Gaussian fitting for the emission spectrum of transition from ${}^4F_{9/2}$ to ${}^6H_{15/2}$ at 5 K for compound 4	S23
Fig. S34–S36 The emission spectra at 77 K and the Gaussian fitting of for the spectrum of transition from ${}^4F_{9/2}$ to ${}^6H_{15/2}$ for compounds 1–3	S24–S25
Fig. S37 The emission spectra at 77 K for compounds 5–8	S25
Fig. S38 The fine spectra from 10 to 50 K for compound 8	S26
Fig. S39 The emission spectra under weak pulse magnetic field for compound 4	S26
Fig. S40 The luminescence spectra of the transitions of ${}^4F_{9/2} \rightarrow {}^6H_{13/2}$ and ${}^4F_{9/2} \rightarrow {}^6H_{15/2}$ under the high pulse magnetic field for compound 4	S27
Fig. S41 The emission spectra of transition from ${}^4F_{9/2}$ to ${}^6H_{15/2}$ under 4–7 T for compound 4	S28
Fig. S42 The parts of each emission spectra under the pulse magnetic field of 11–36 T for compound 4	S29–S30
Fig. S43–S46 The energy levels for the magnetic low-lying states of the ground term obtained by variable methods and the magntic easy axes for 1–4 and 8	S31–S33
Table S1. Elemental analysis for sublimed samples 5–8	S34
Table S2–S6. Crystallographic data and structure refinements for compounds 1–4 and 8	S35–S39
Table S7 The coordination bond length of Dy–O and Dy–N for compounds 1–4 and 8	S40
Table S8 The bond angles of Dy for 4 and 8	S41–S42
Table S9 The summary the parameters of the dynamic magnetic relaxation	S43
Table S10–S14 Gaussian components from fitting the luminescence spectra for compounds 1–4 and 8	S43–S44
Table S15–S16 The values of E and g for compounds compounds 1–4 and 8	S45–S46
Table S17 The wave functions of the ground and first excited states of the term ${}^6H_{15/2}$ of 4	S46

The IR data for compounds **2–7**

Reference

S47

S47

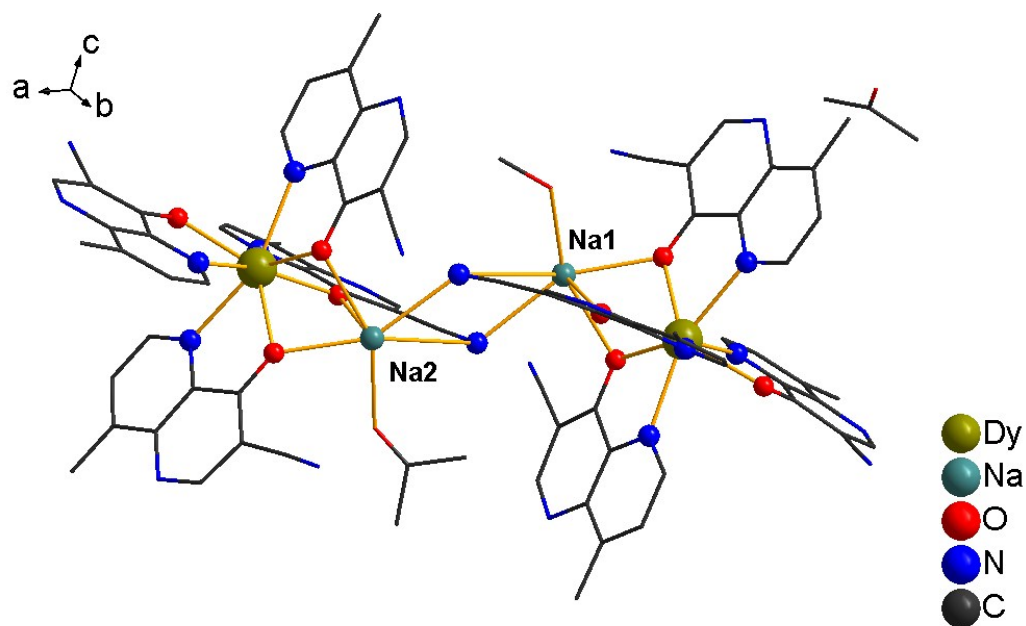


Fig. S1 The molecular structure of the $\{DyNa\}$ (1).

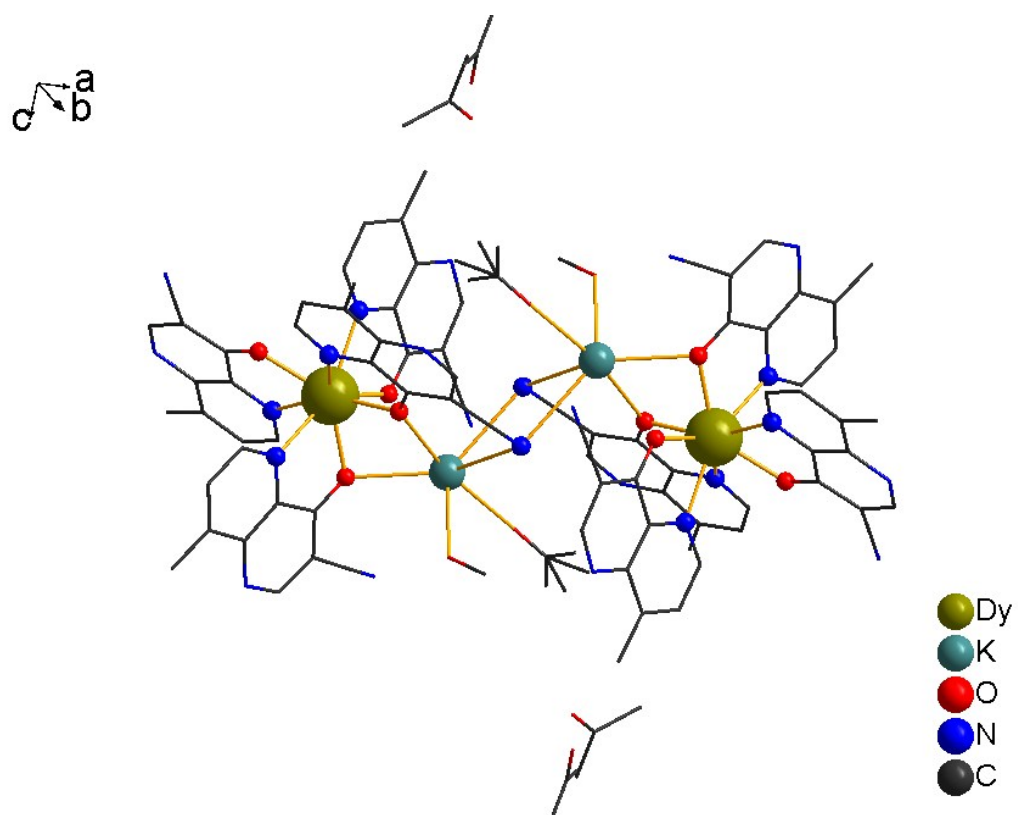


Fig. S2 The molecular structure of the $\{DyK\}$ (2). The disorder of the lattice solvent of acetone for compounds **2** is treated with the 53% and 47% occupancy respectively.

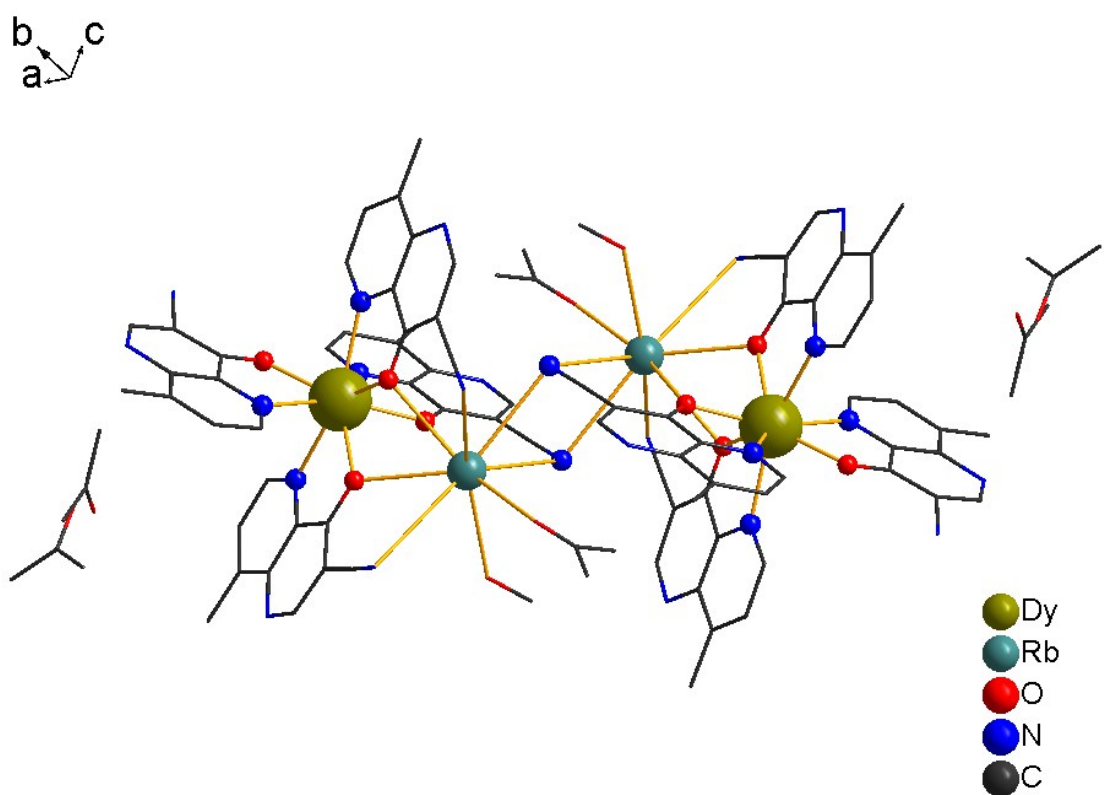


Fig. S3 The molecular structure of the {DyRb} (**3**). The disorder of the lattice solvent of acetone for compounds **3** is treated with the 59% and 41% occupancy respectively.

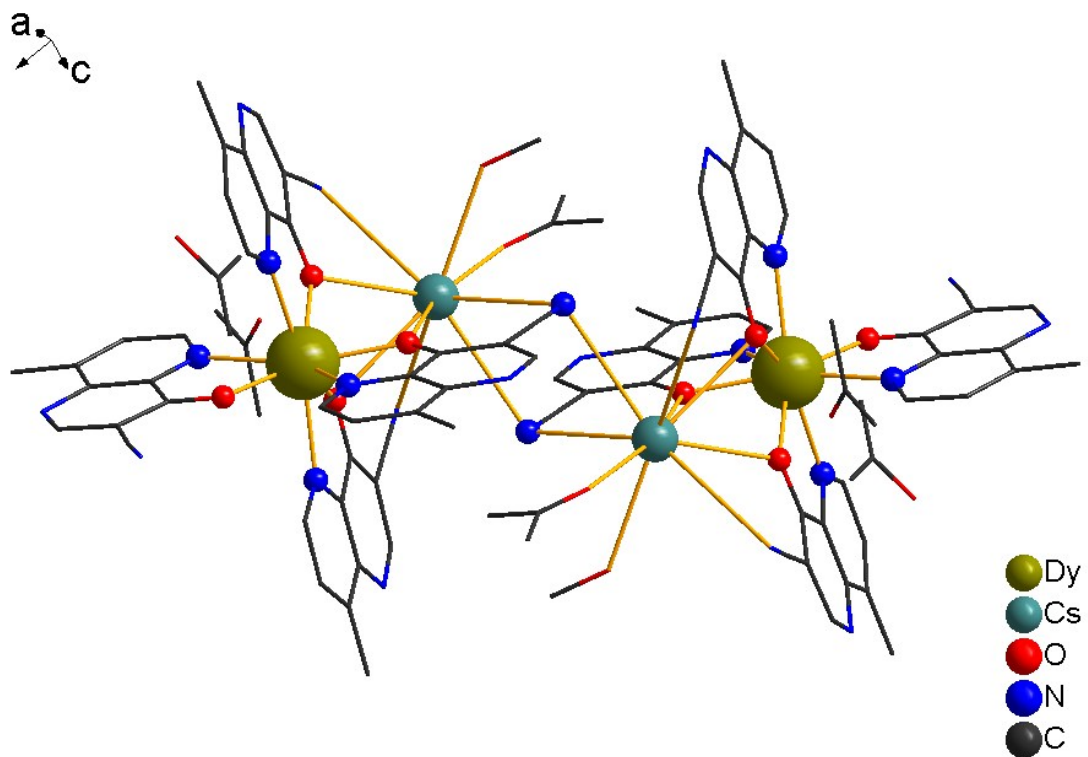


Fig. S4 The molecular structure of the {DyCs} (**4**). The disorder of the lattice solvent of acetone for compounds **4** is treated with the 50% and 50% occupancy respectively.

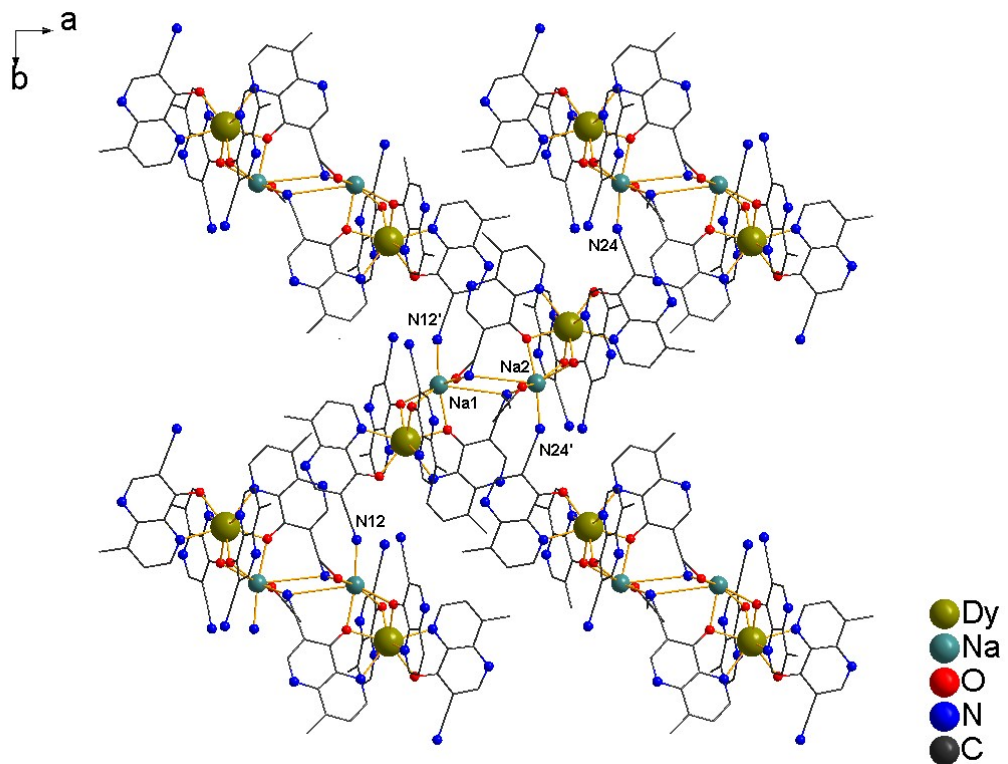


Fig. S5 The packing diagram along c axis for $\{ \text{DyNa} \}$ (**1**). The interaction of Na (Na1, Na2) atoms with N atoms (N12', N24') from adjacent molecules and the interaction of N atoms (N12, N24) with Na atoms in nearby molecule extend the compound in the ab plane.

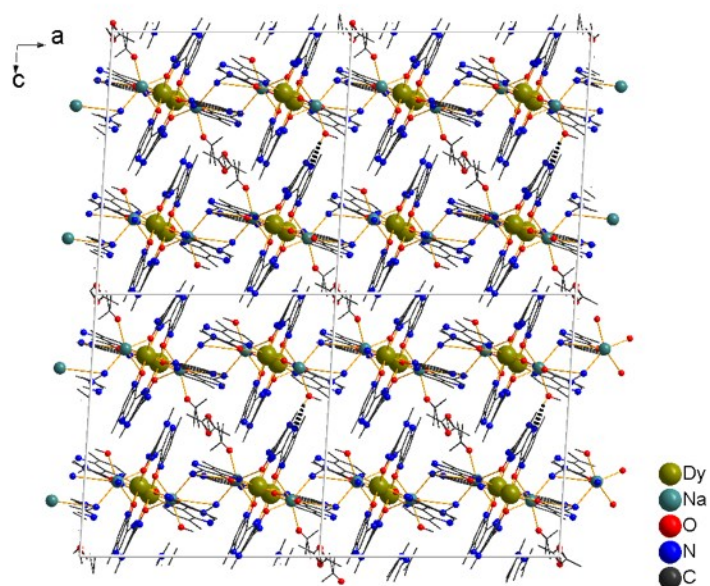


Fig. S6 The packing diagram along b axis for $\{ \text{DyNa} \}$ (**1**). The black dashed lines represent the H bonds. The H bond and $\pi-\pi$ stacking along c axis connected the sheets in ab plane.

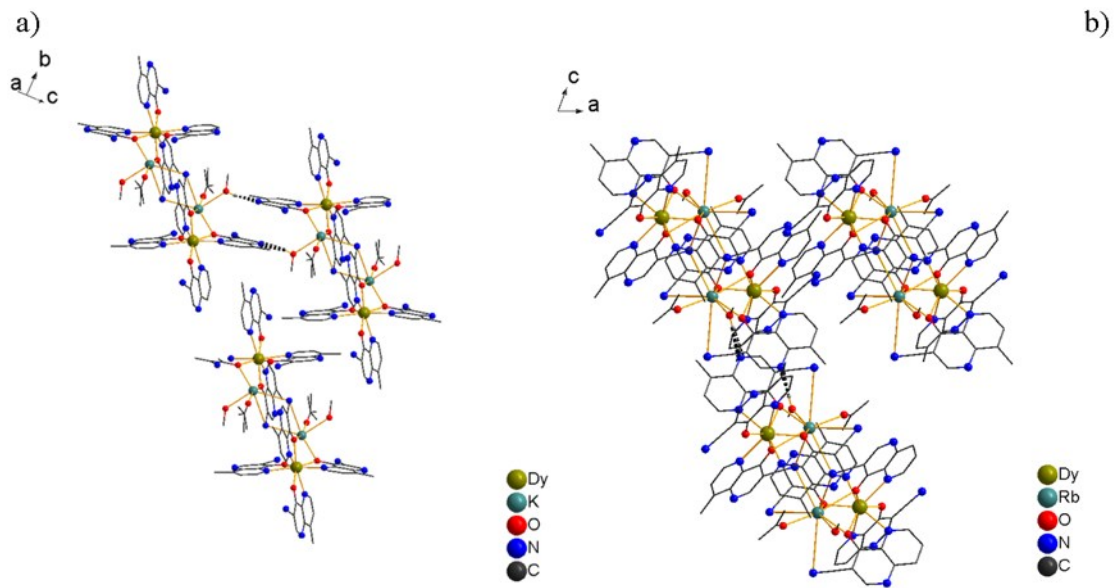


Fig. S7 (a) The packing diagram for $\{\text{DyK}\}$ (**2**); (b) The packing diagram for $\{\text{DyRb}\}$ (**3**). The black dashed lines represent the H bonds. And the $\pi-\pi$ stacking is interacted between molecules along *b* and *a* axes for **2** and **3** respectively.

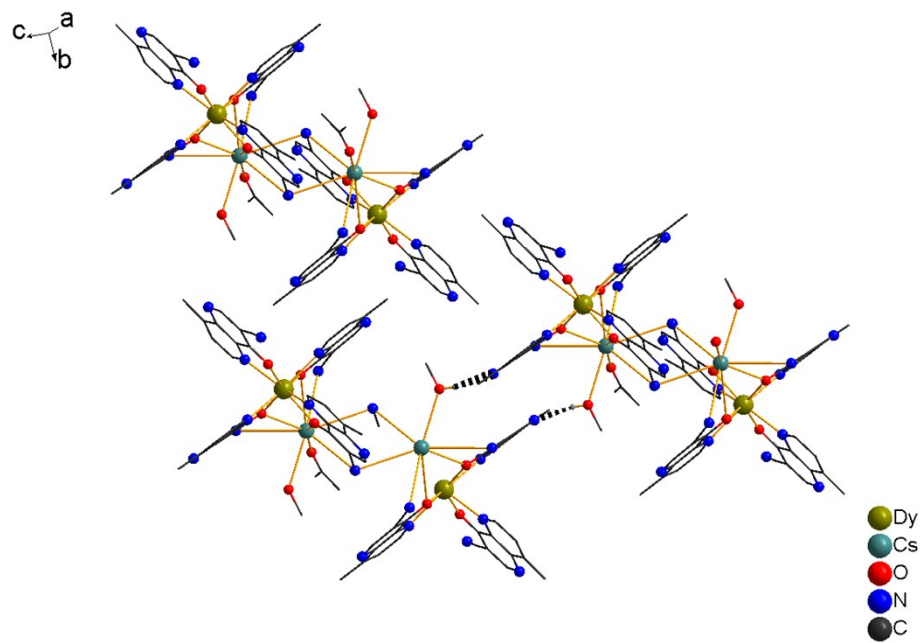


Fig. S8 The packing diagram for $\{\text{DyCs}\}$ (**4**). The black dashed lines represent the H bonds. And the $\pi-\pi$ stacking is interacted between molecules in two directions.

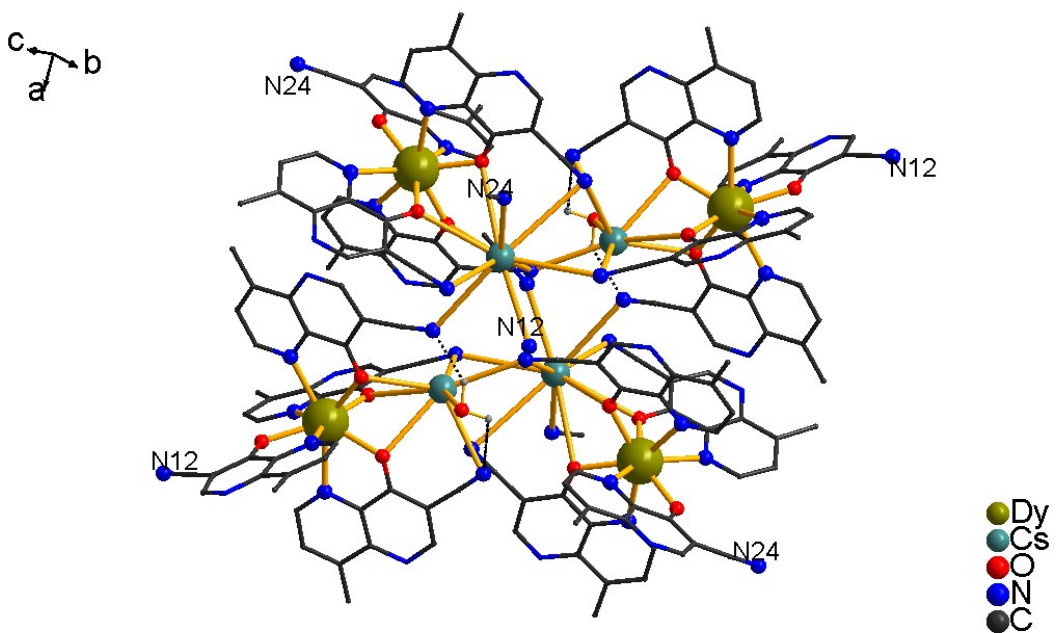


Fig. S9 The molecular structure of the $\{DyCs\}_{sub}$ (8). The black dashed lines represent the H bonds.

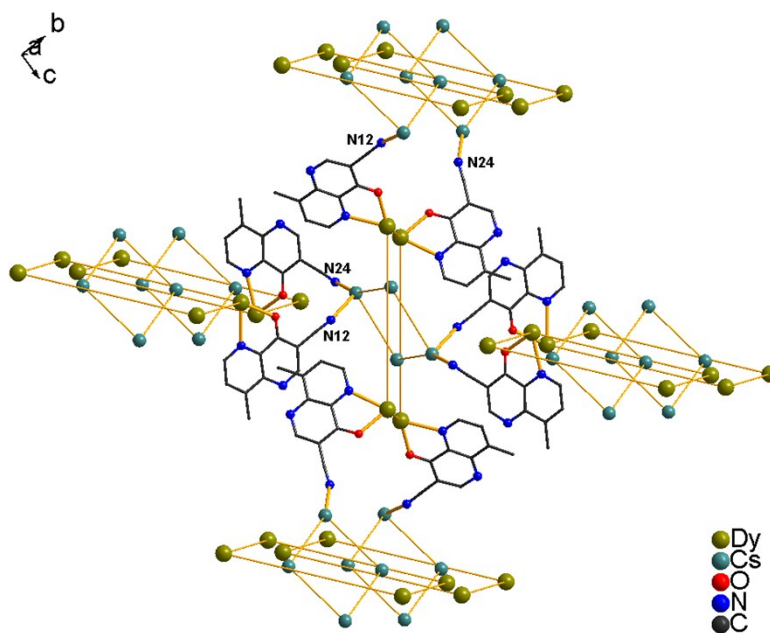
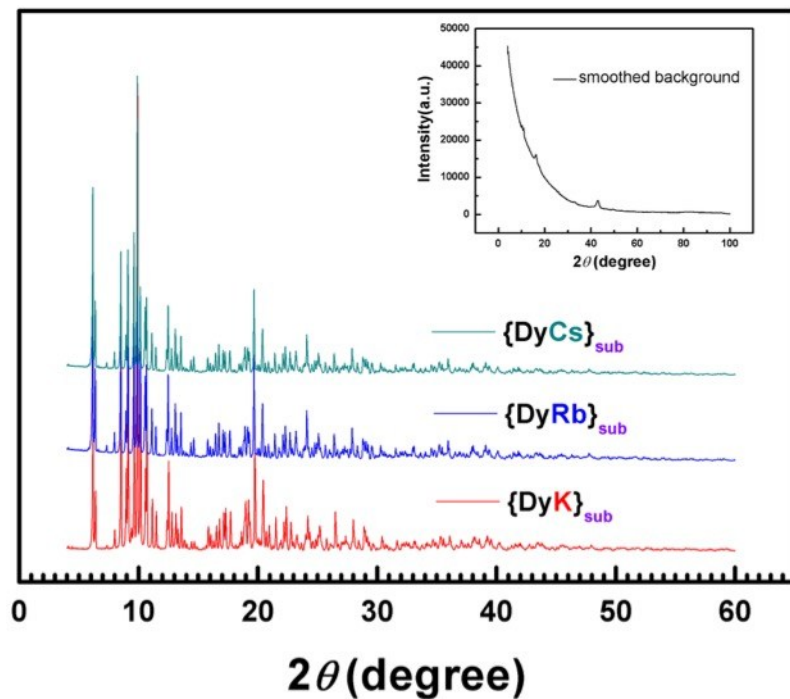


Fig. S10 The packing diagram is for $\{DyCs\}_{sub}$ (8). The thin yellow lines between metal ions are just for eye guide to recognize the huge molecule. The molecule in center extended into 3 dimensions by the interaction between N atom from cyan group and Cs ion.

a)



b)

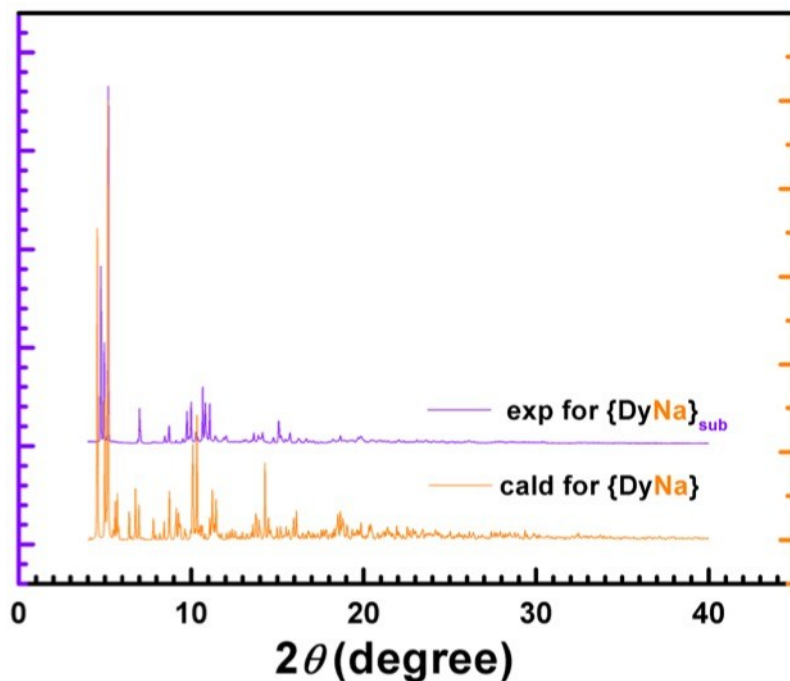
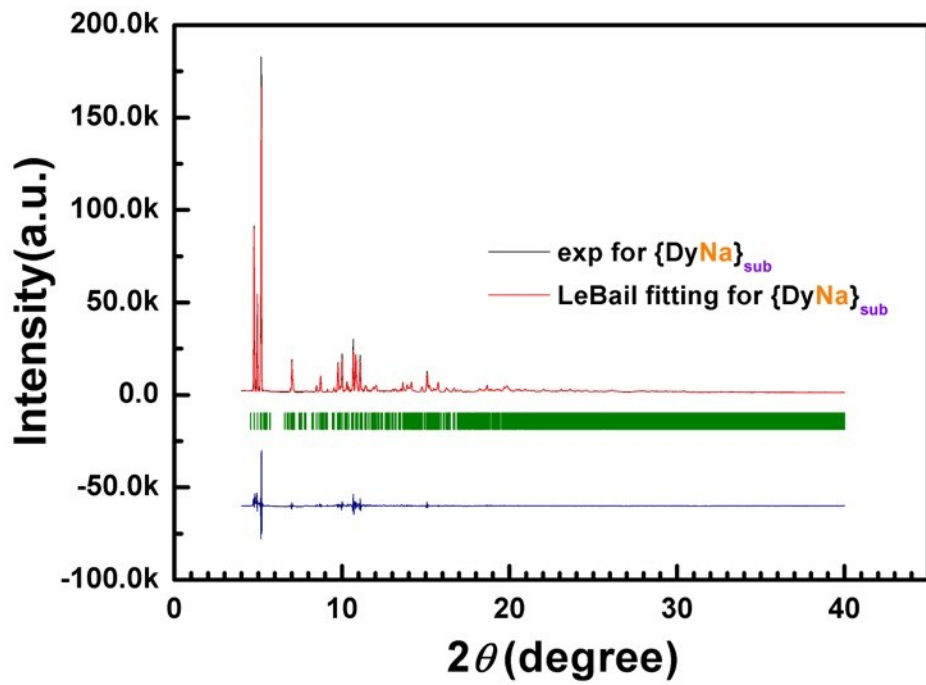
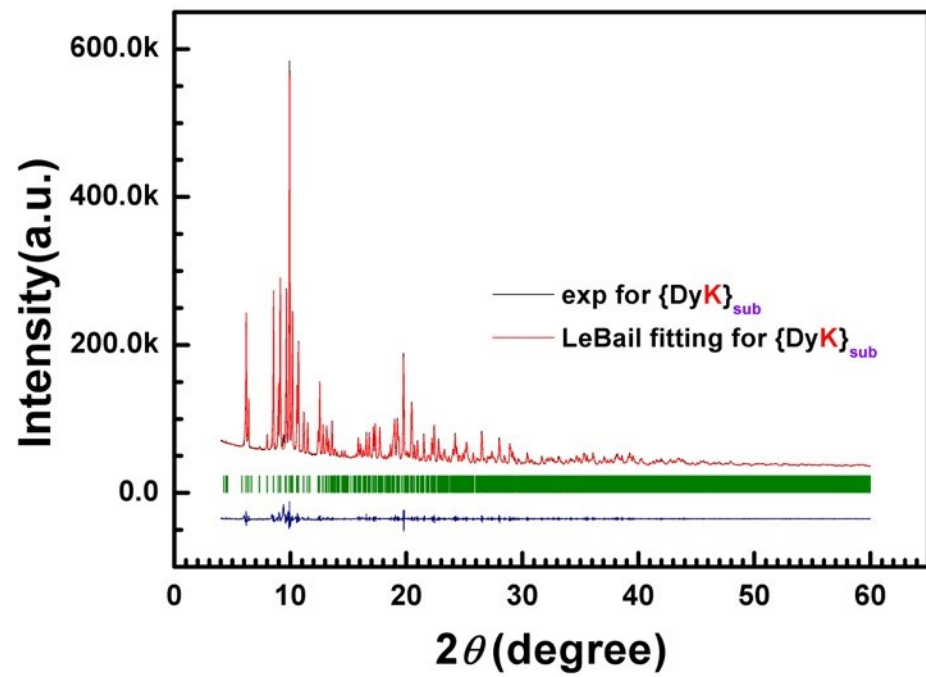


Fig. S11 (a) The simulated and experimental powder X-ray diffraction patterns of $\{DyK\}_{sub}$ (6) and $\{DyRb\}_{sub}$ (7) are compared to the one of $\{DyCs\}_{sub}$ (8). Inset shows the background curve smoothed. (b) The pxrd plots for $\{DyNa\}$ (1) and $\{DyNa\}_{sub}$ (5) are described and the apparent difference are shown.

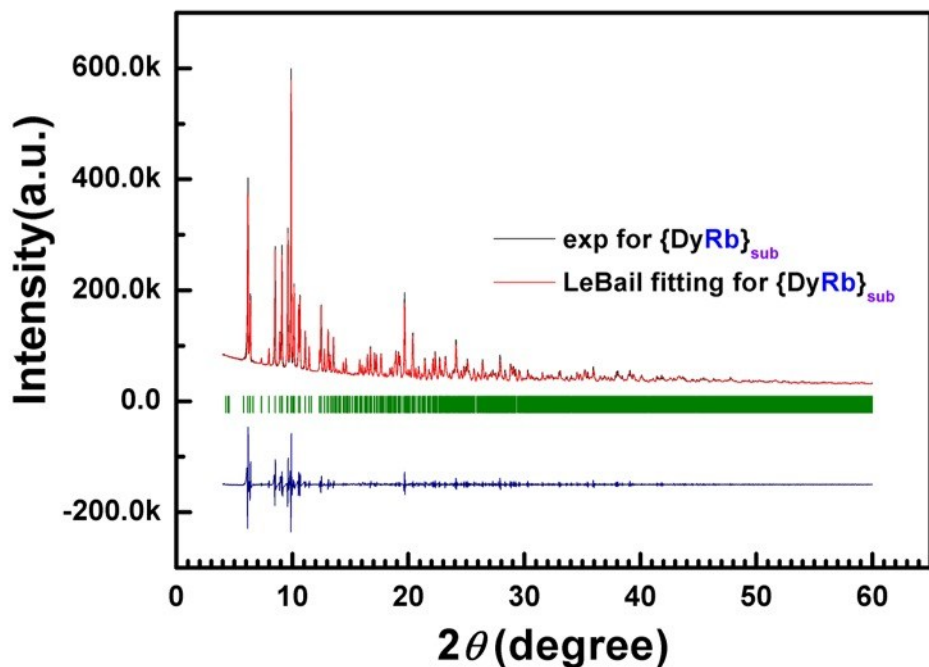
(a)



(b)



(c)



(d)

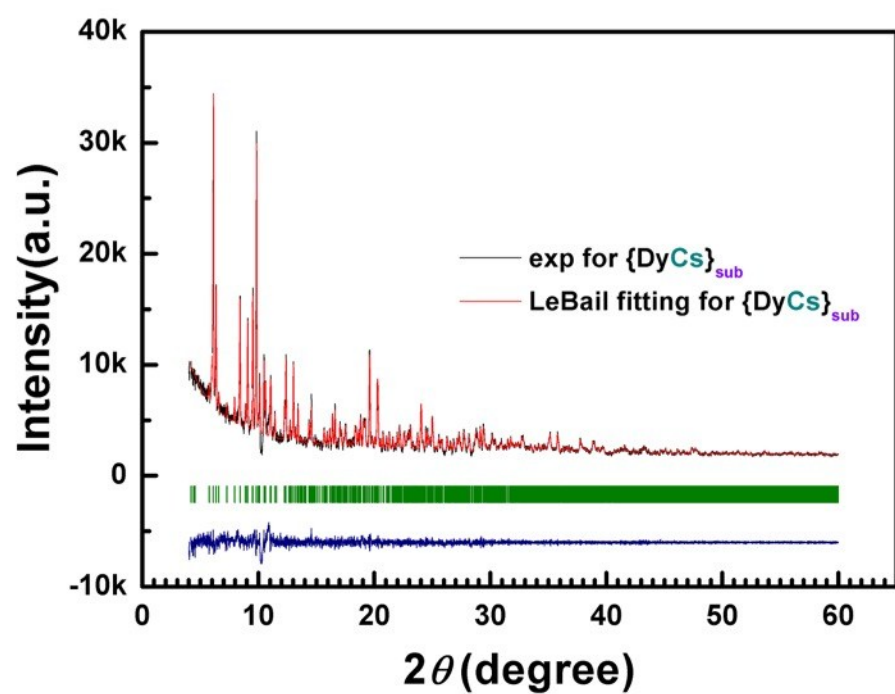


Fig. S12 (a)–(d) LeBail fitting for compounds $\{\text{DyNa}\}_{\text{sub}}$ (**5**), $\{\text{DyK}\}_{\text{sub}}$ (**6**), $\{\text{DyRb}\}_{\text{sub}}$ (**7**), and $\{\text{DyCs}\}_{\text{sub}}$ (**8**). Navy lines represent the intensity difference between the observed and fitted values. Olive lines denote the peak indexes.

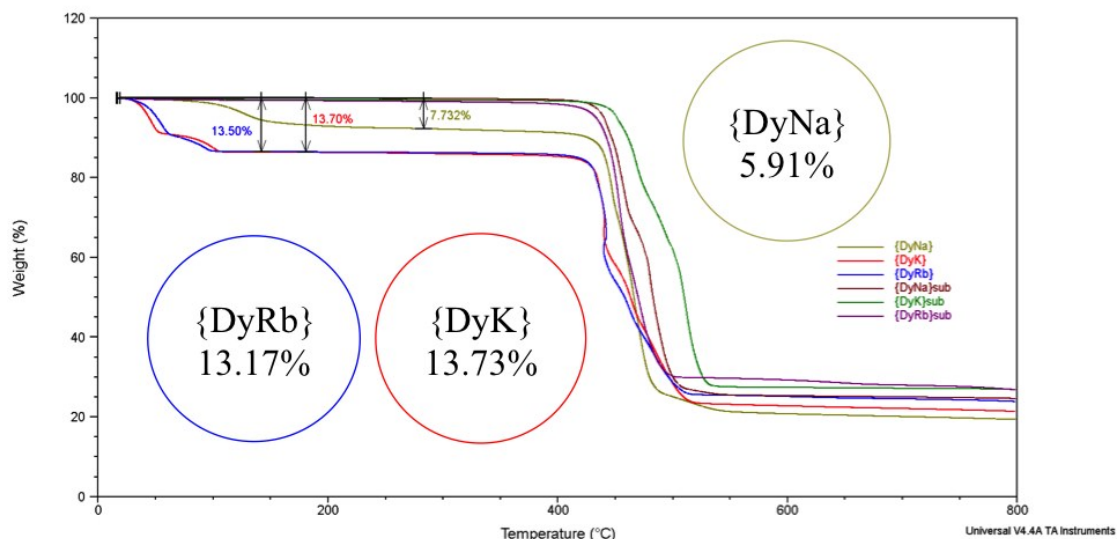


Fig. S13 The thermogravimetry curve states the stability while heating for compound {DyNa} (**1**), {DyK} (**2**), {DyRb} (**3**) and {DyNa}_{sub} (**5**), {DyK}_{sub} (**6**), {DyRb}_{sub} (**7**); Insets show the calculated mass percentage of the whole solvents in a molecule. The traces of lost gravity in the range from room temperature to 200 and 300 °C are 0.1267 % and 0.5429 % (**5**), 0.5510 % and 0.6352 % (**6**), 0.7364% and 0.9835 % (**7**), respectively. This loss of gravity might be ascribed to the coordinated and adsorbed water.

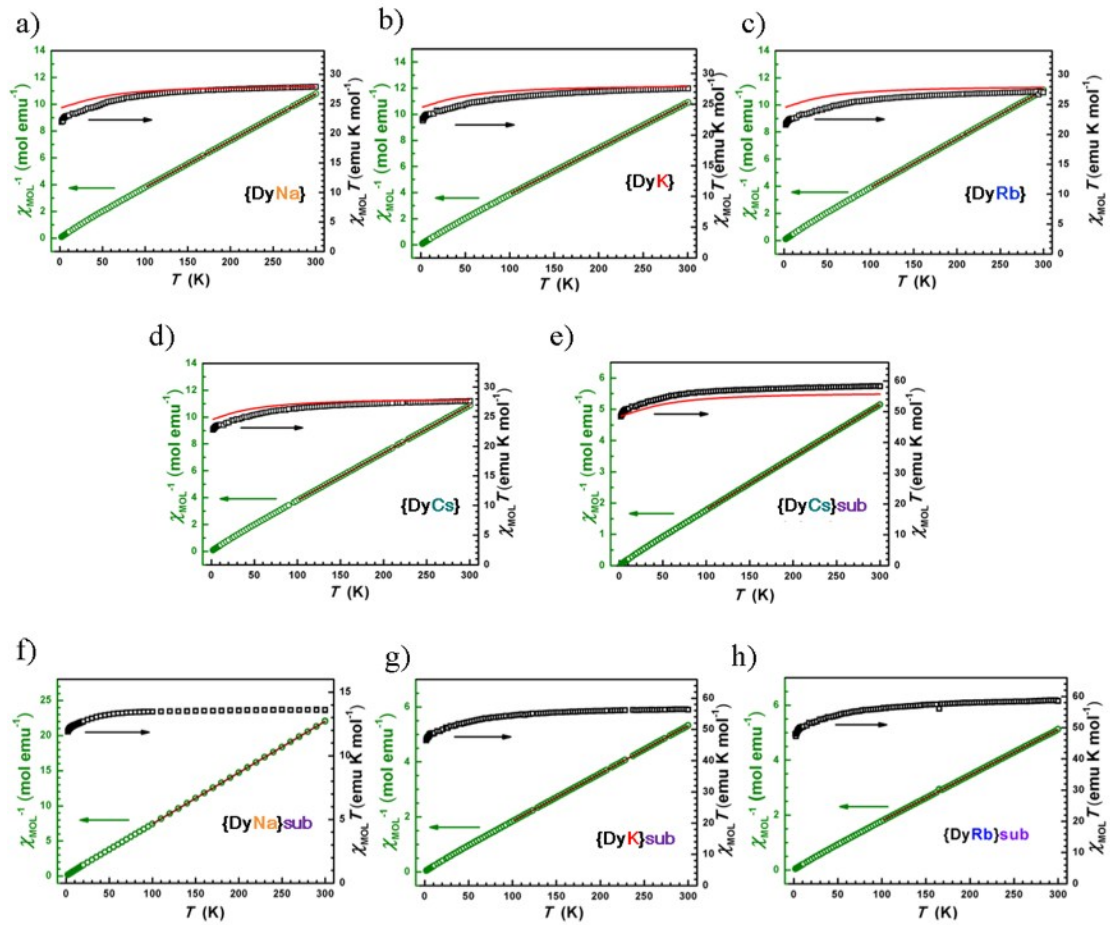


Fig. S14 (a)–(h) The plots of χ_{M}^{-1} vs. T are fitted by Curie–Weiss formula (wine lines, C and θ = 28.62 and -8.41 for {DyNa} (**1**), 28.43 and -9.78 for {DyK} (**2**), 27.82 and -8.32 for {DyRb} (**3**), 28.30 and -7.64 for {DyCs} (**4**), 13.69 and -1.75 for {DyNa}_{sub} (**5**), 57.50 and -5.35 for {DyK}_{sub} (**6**), 60.10 and -7.45 for {DyRb}_{sub} (**7**), 59.31 and -5.56 for {DyCs}_{sub} (**8**)). The sign of indicates the possible antiferromagnetic interaction. $\chi_{\text{M}} T$ values from experiment and CASSCF calculation (red lines) are compared for compounds **1–4** and **8**.

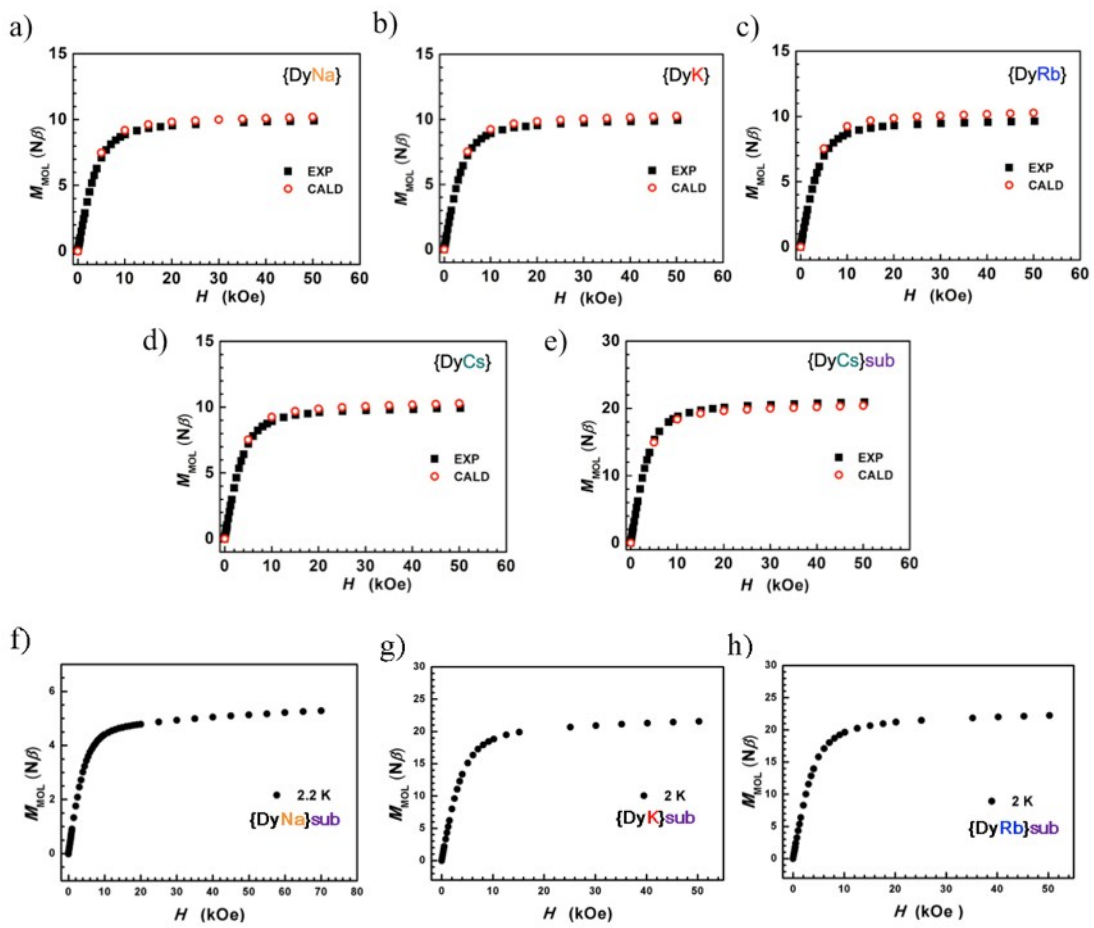


Fig. S15 (a)–(e) The magnetization *vs.* magnetic field at 2 K from experiment and CASSCF calculation are agreed well for **1–4** and **8**. (f)–(h) The magnetization *vs.* magnetic field at 2.2 K for $\{\text{DyNa}\}_{\text{sub}}$ (**5**) and 2 K for $\{\text{DyK}\}_{\text{sub}}$ (**6**) and $\{\text{DyRb}\}_{\text{sub}}$ (**7**).

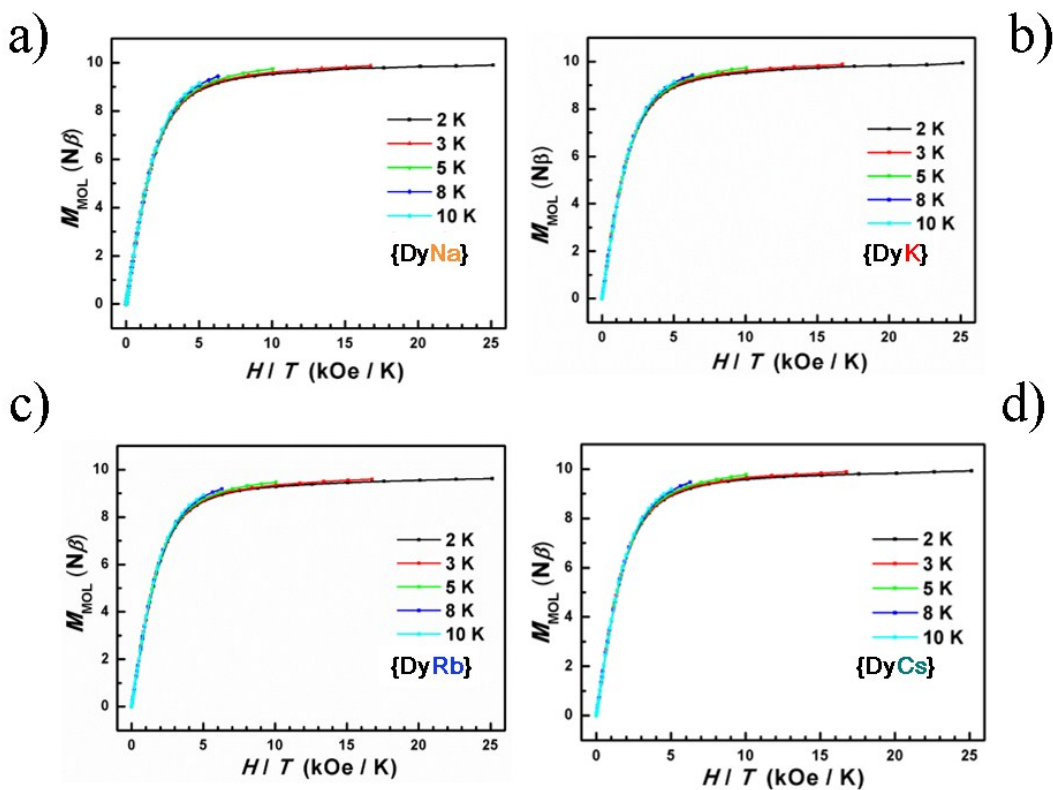


Fig. S16 (a)–(d) The plots of magnetization *vs.* the product of H and T^{-1} for four compounds of $\{DyNa\}$ (1), $\{DyK\}$ (2), $\{DyRb\}$ (3), and $\{DyCs\}$ (4).

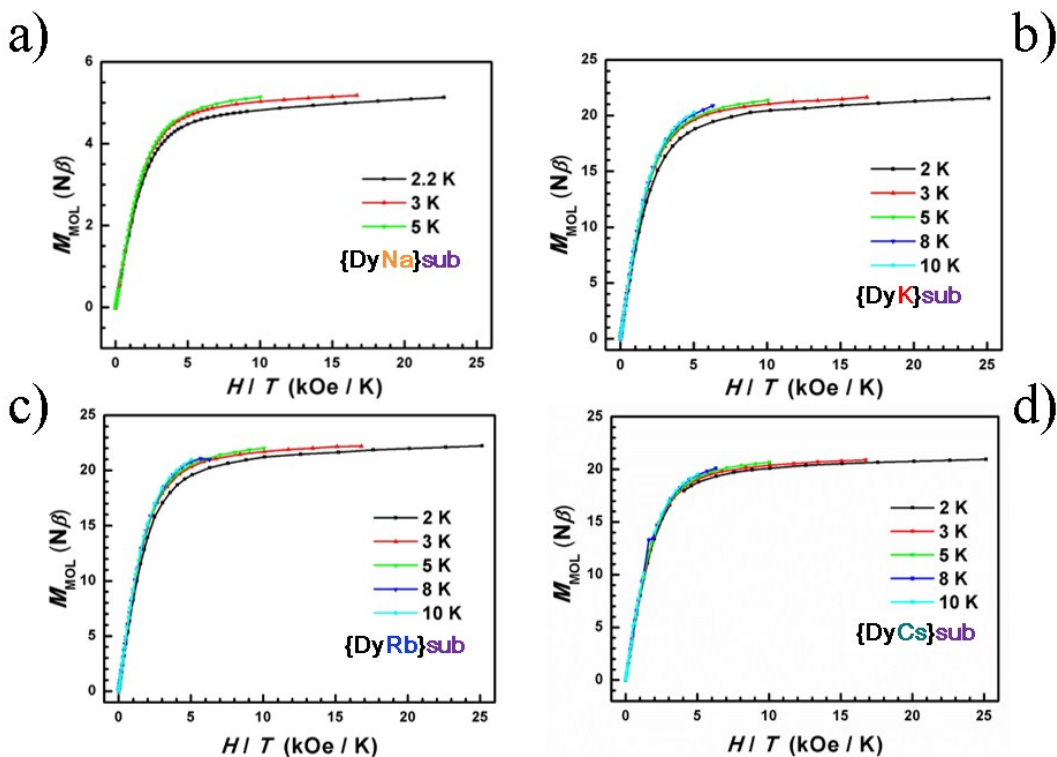


Fig. S17 (a)–(d) The plots of magnetization *vs.* the product of H and T^{-1} for four sublimed samples $\{DyNa\}_{sub}$ (5), $\{DyK\}_{sub}$ (6), $\{DyRb\}_{sub}$ (7), and $\{DyCs\}_{sub}$ (8).

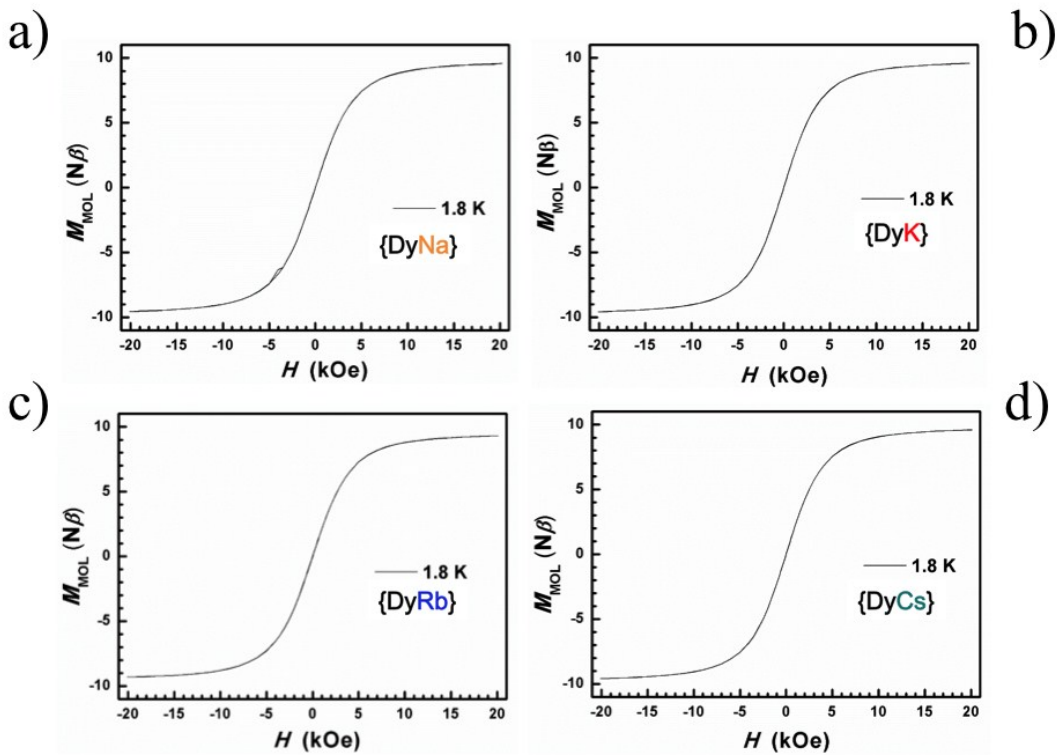


Fig. S18 (a)–(d) The magnetic hysteresis curves at 1.8 K for compounds of {DyNa} (1), {DyK} (1), {DyRb} (3), and {DyCs} (4).

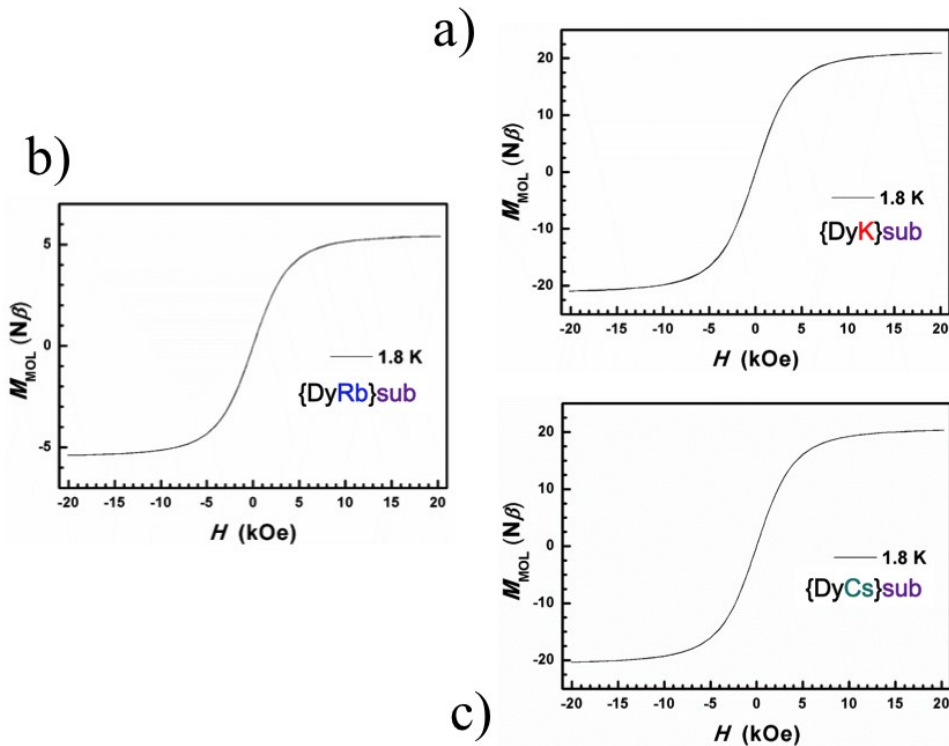


Fig. S19 (a)–(c) The magnetic hysteresis curves for compounds of {DyK}_{sub} (6), {DyRb}_{sub} (7), {DyCs}_{sub} (8).

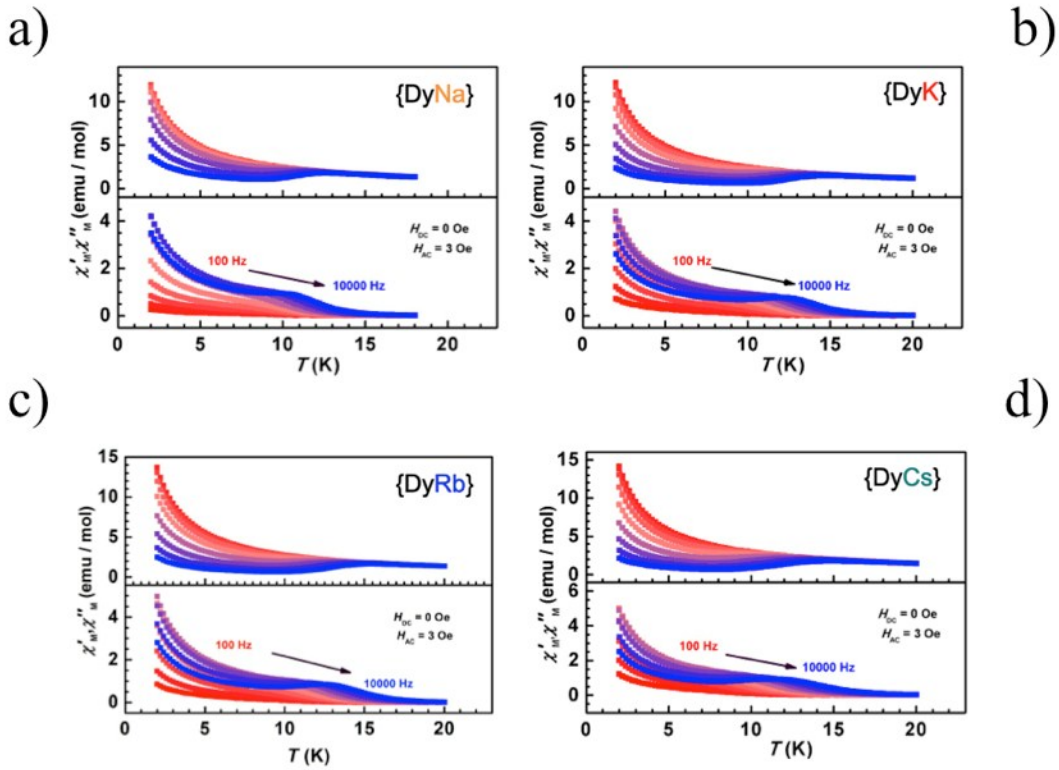


Fig. S20 (a)–(d) The plots of ac magnetic susceptibilities versus T at temperature range of 2–20 K for compounds of {DyK} (2), {DyRb} (3), and {DyCs} (4), but the narrow range for {DyNa} (1).

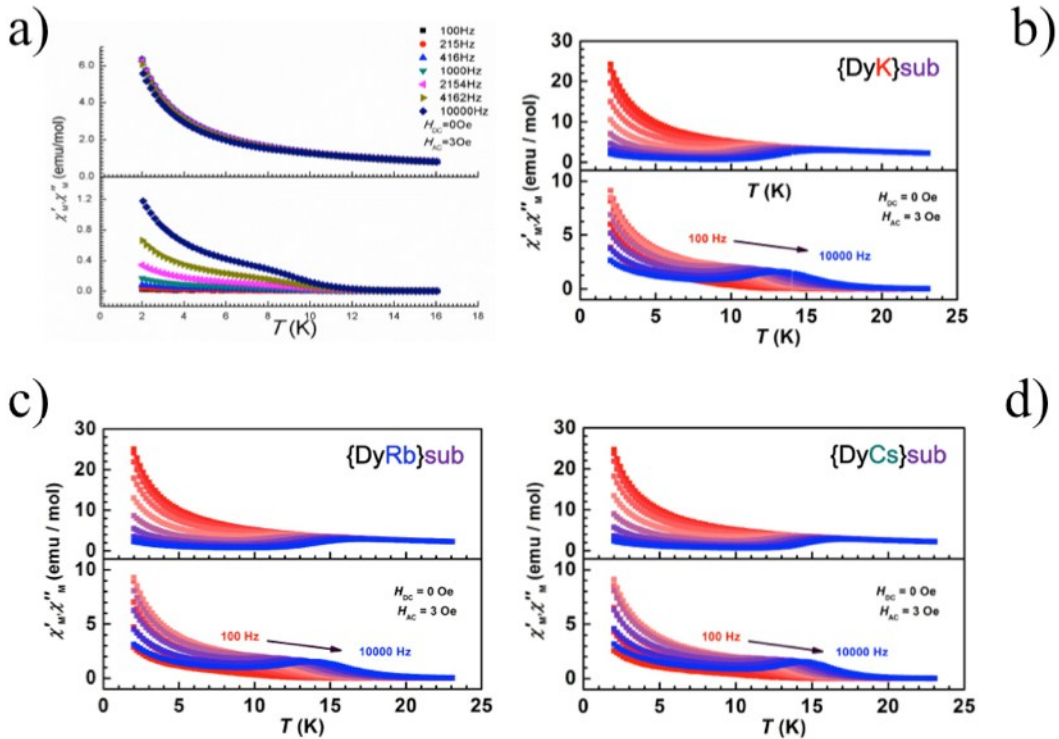


Fig. S21 (a)–(d) The plots of ac magnetic susceptibilities versus T at temperature range of 2–20 K for compounds of {DyK}_{sub} (6), {DyRb}_{sub} (7), {DyCs}_{sub} (8), but the narrow range for {DyNa}_{sub} (5).

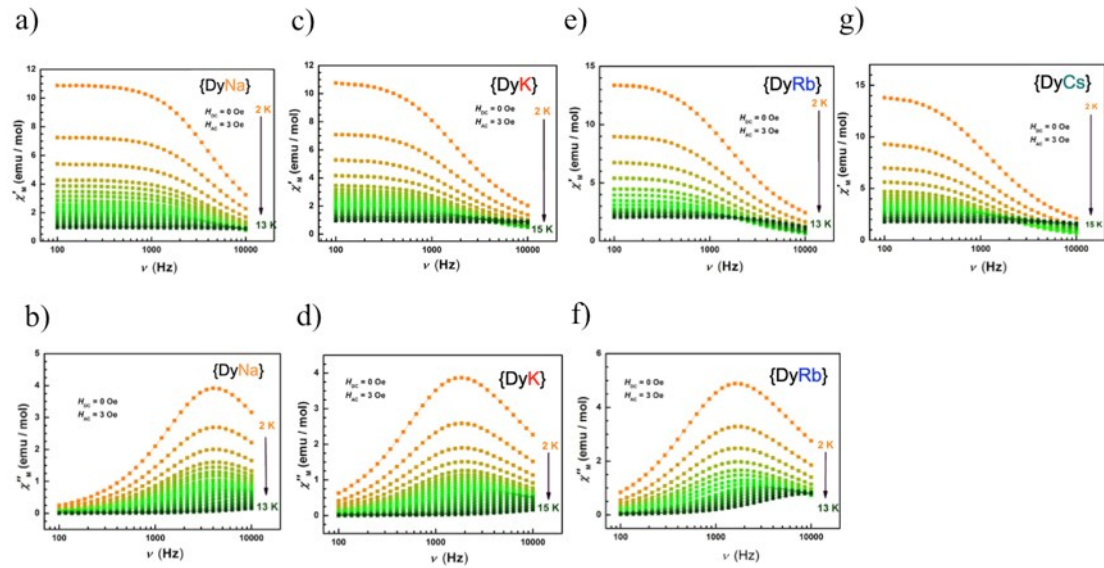


Fig. S22 (a)–(f) The in-phase and out-of-phase of the AC magnetic susceptibilities at different temperature for compounds {DyNa} (1), {DyK} (2), {DyRb} (3); (g) The in-phase of the AC magnetic susceptibilities at different temperature for compound {DyCs} (4).

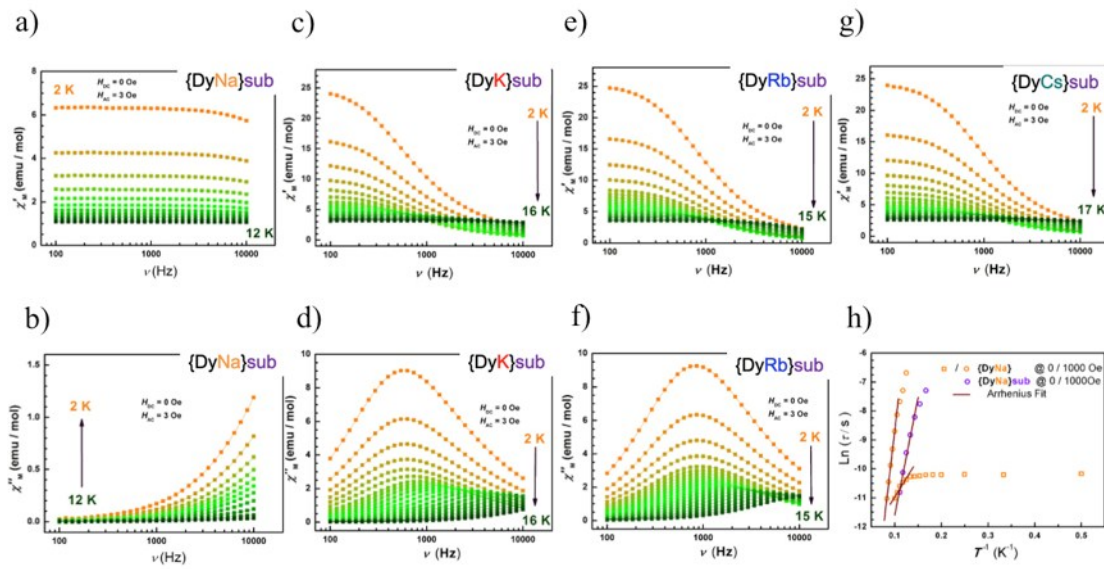


Fig. S23 (a)–(g) The in-phase and out-of-phase of the AC magnetic susceptibilities at different temperature for compounds {DyNa}_{sub} (5), {DyK}_{sub} (6), {DyRb}_{sub} (7), and {DyCs}_{sub} (8); (h) The Arrhenius fit for {DyNa} (1) and {DyNa}sub.

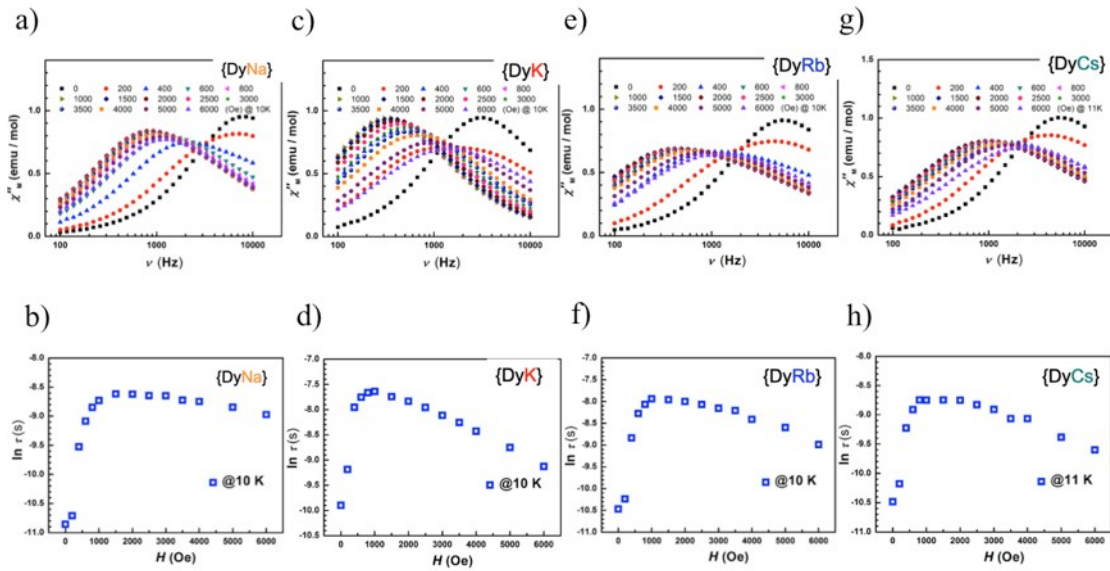


Fig. S24 (a)–(h) The optimization of the external magnetic field for compounds {DyNa} (**1**), {DyK} (**2**), {DyRb} (**3**), and {DyCs} (**4**).

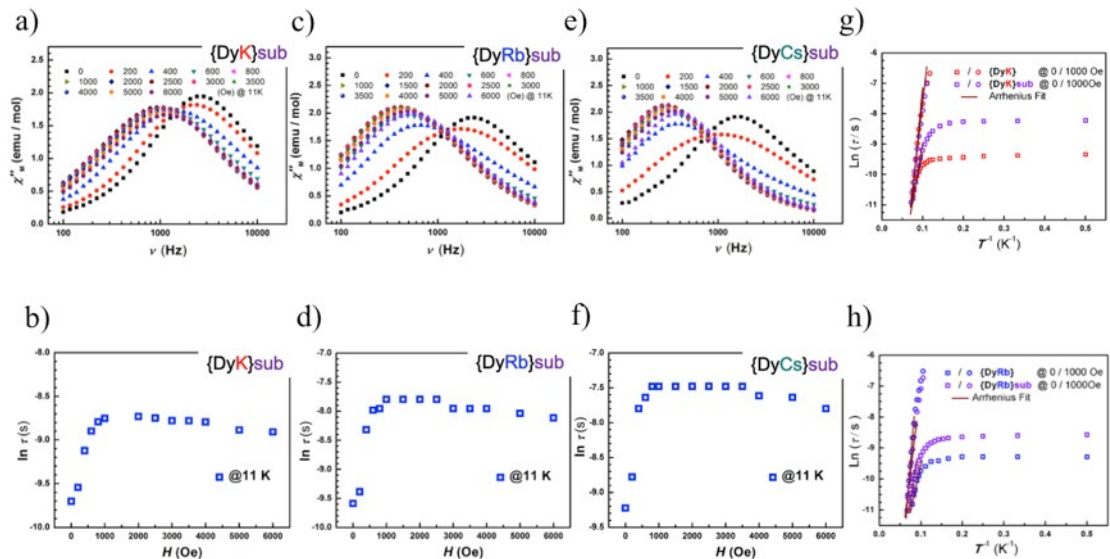


Fig. S25 (a)–(f) The optimization of the external magnetic field for compounds {DyNa} sub (**5**), {DyK} sub (**6**), {DyRb} sub (**7**); (g)–(h) The Arrhenius fit for {DyK} (**2**), {DyK} sub (**6**) and {DyRb} (**3**), {DyRb} sub (**7**).

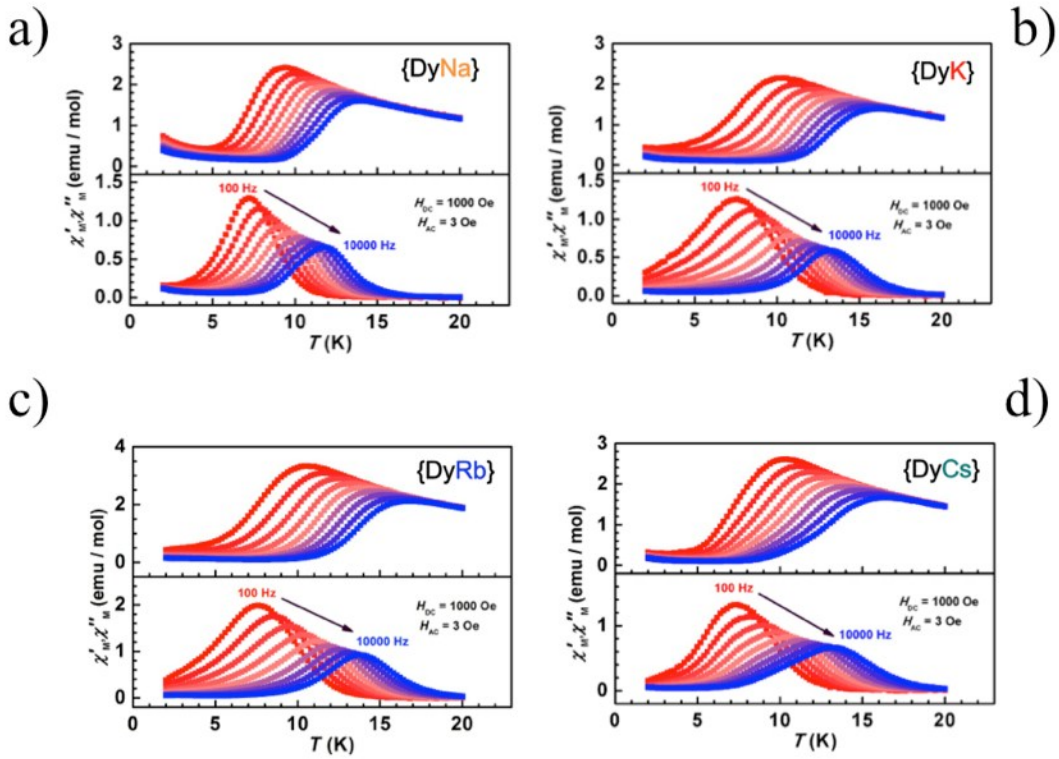


Fig. S26 (a)–(d) The plots of ac magnetic susceptibilities under a DC field of 1000 Oe versus T at temperature range of 2–20 K for compounds of {DyNa} (1), {DyK} (2), {DyRb} (3), and {DyCs} (4).

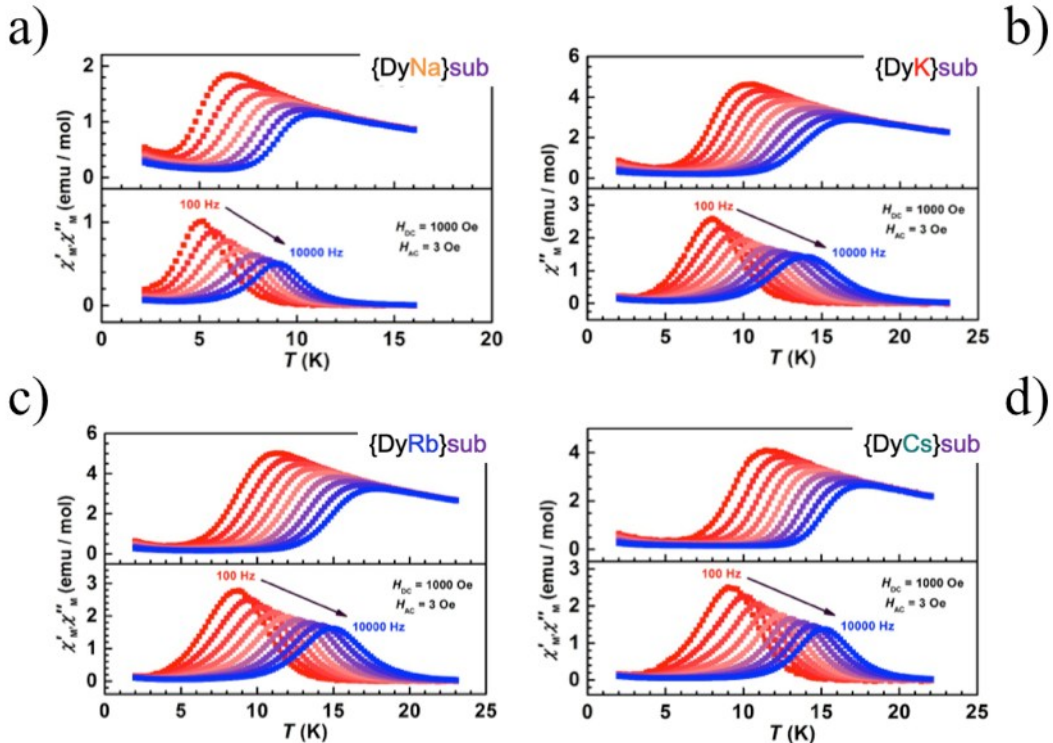


Fig. S27 (a)–(d) The plots of ac magnetic susceptibilities under a DC field of 1000 Oe versus T at temperature range of 2–20 K for compounds of {DyNa}_{sub} (5), {DyK}_{sub} (6), {DyRb}_{sub} (7), and {DyCs}_{sub} (8).

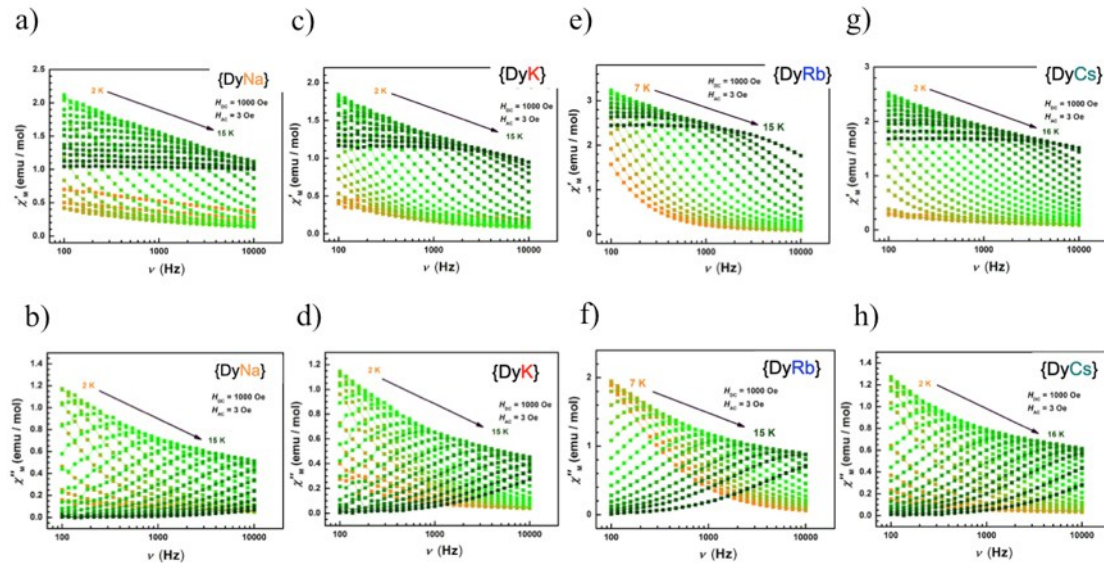


Fig. S28 (a)–(h) The in-phase and out-of-phase of the AC magnetic susceptibilities under a DC field of 1000 Oe at different temperature for compounds {DyNa} (1), {DyK} (2), {DyRb} (3), and {DyCs} (4).

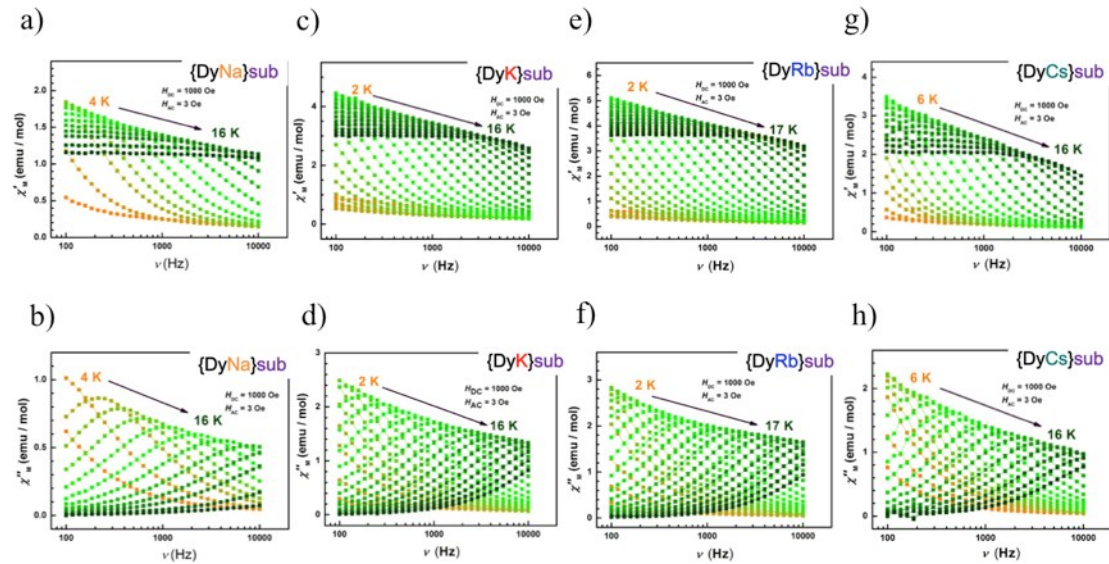


Fig. S29 (a)–(h) The in-phase and out-of-phase of the AC magnetic susceptibilities under a DC field of 1000 Oe at different temperature for compounds {DyNa}sub (5), {DyK}sub (6), {DyRb}sub (7), and {DyCs}sub (8).

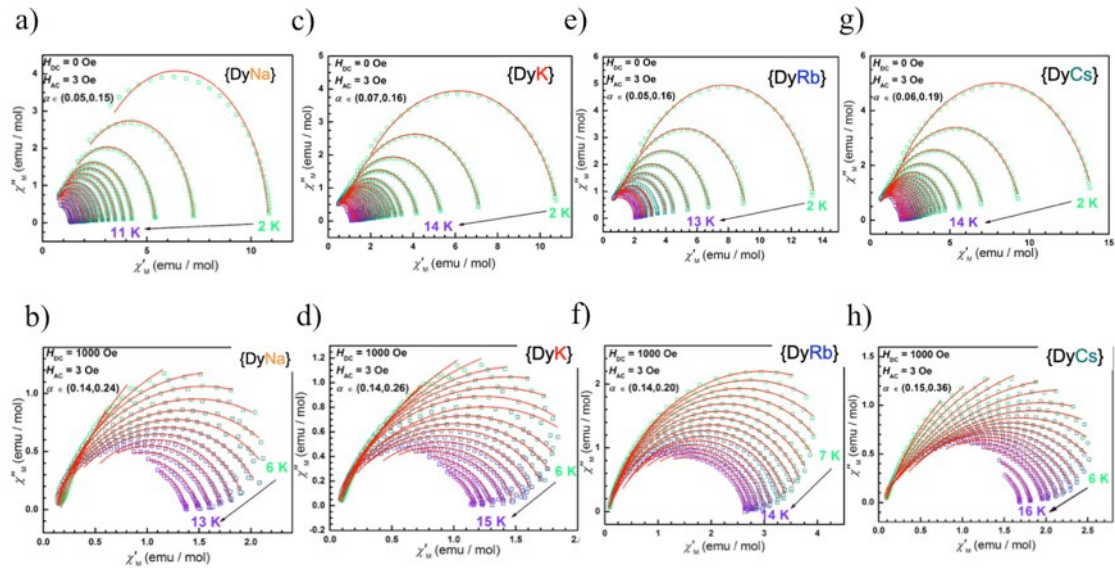


Fig. S30 (a)–(h) The Cole-Cole fitting under static magnetic field of 0 and 1000 Oe for compounds {DyNa} (1), {DyK} (2), {DyRb} (3), and {DyCs} (4).

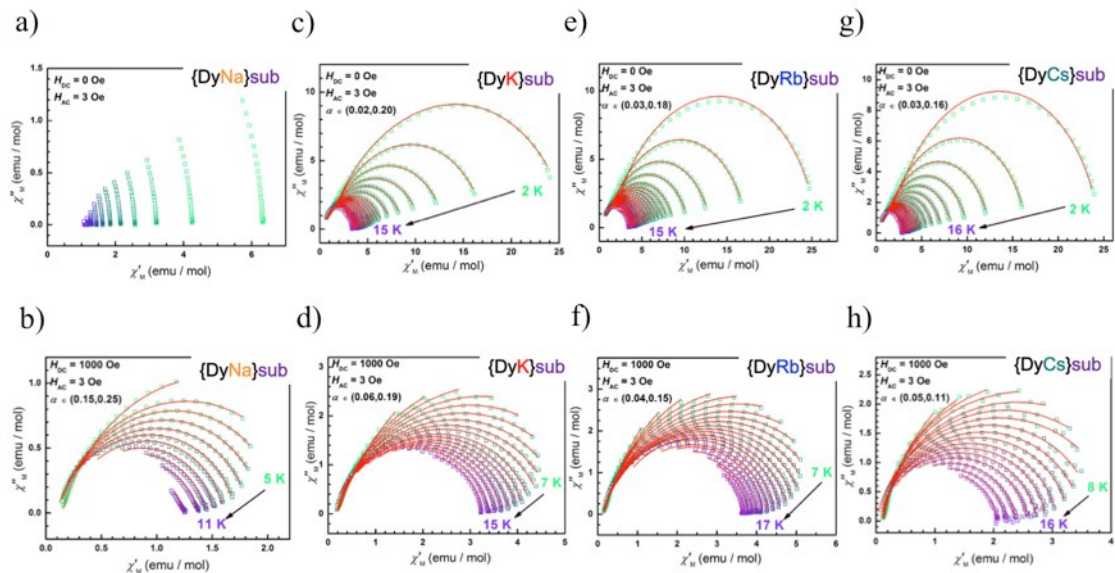


Fig. S31 (b)–(h) The Cole-Cole fitting under static magnetic field of 0 and 1000 Oe for compounds {DyNa}sub (5), {DyK}sub (6), {DyRb}sub (7), and {DyCs}sub (8); (a) The data of {DyNa}sub at 0 Oe could not be fitted.

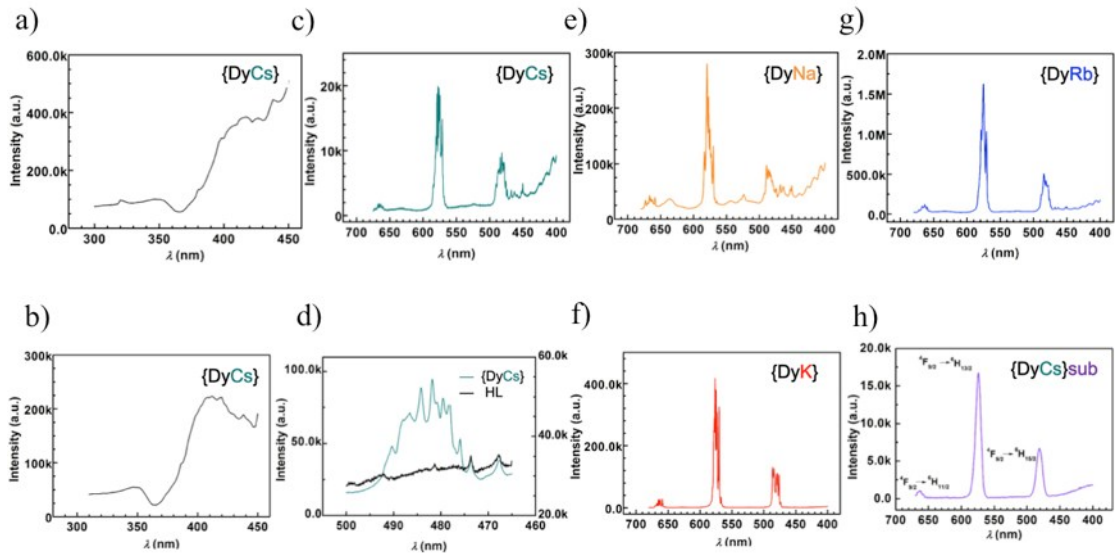


Fig. S32 (a) The excited spectrum for $\{\text{DyCs}\}$ (**4**) is recorded when fixed the λ_{em} on 485 nm. (b) The excited spectrum for $\{\text{DyCs}\}$ is recorded when fixed the λ_{em} on 575 nm. (c)–(g) The emission spectra are obtained for compounds $\{\text{DyNa}\}$ (**1**), $\{\text{DyK}\}$ (**2**), $\{\text{DyRb}\}$ (**3**), and $\{\text{DyCs}\}$, with the fine spectrum (d) compared with the background of the ligand emission. (h) The picosecond pulse light emitting diode at 340 ± 10 nm is employed as quasi-continuous light source and Dy emission for $\{\text{DyCs}\}_{\text{sub}}$ (**8**) is observed in low intensity with vague resolution.

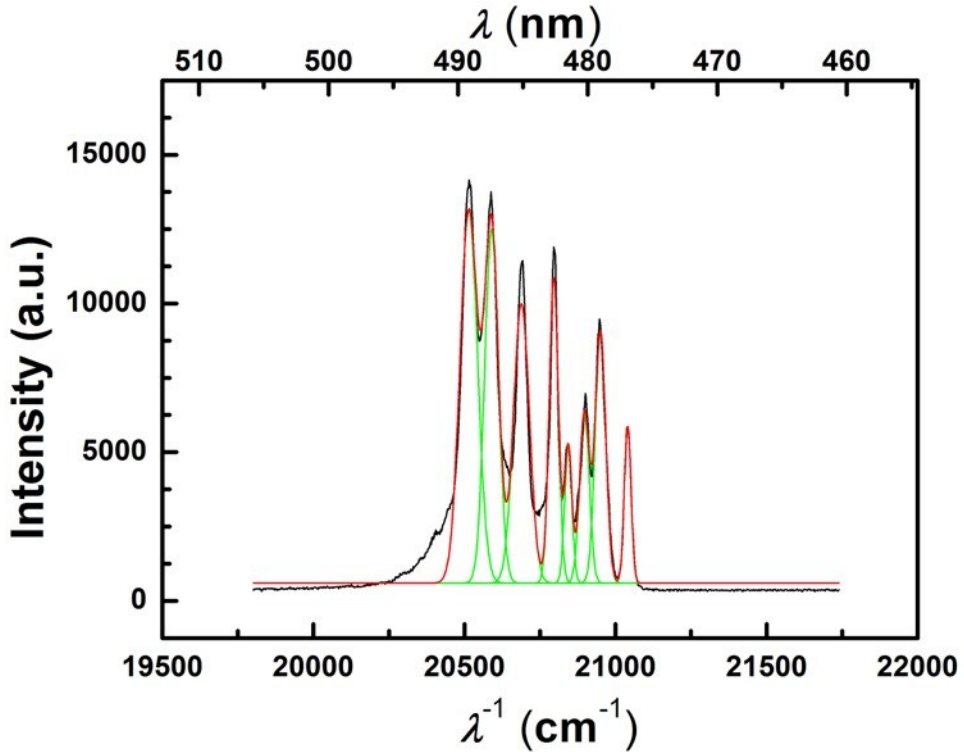


Fig. S33 The Gaussian fitting for the emission spectrum at 5 K within the duration time of 10 ms for $\{\text{DyCs}\}$ (**4**) in the range of 460–505 nm of the transition from ${}^4\text{F}_{9/2}$ to ${}^6\text{H}_{15/2}$.

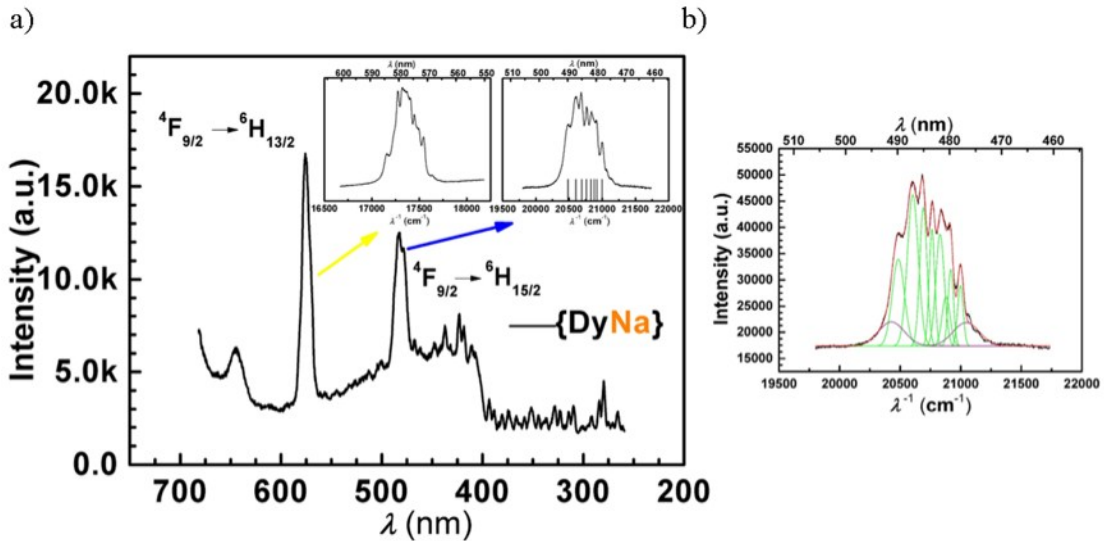


Fig. S34 (a) The emission spectrum at 77 K for $\{\text{DyNa}\}$ (1) in the range of 240–690 nm and the fine spectra of transitions from $^4F_{9/2}$ to $^6H_{13/2}$ and $^6H_{15/2}$ (insets) within the duration time of 10, 50 and 100 ms respectively. (b) The Gaussian fitting for the spectrum of transition from $^4F_{9/2}$ to $^6H_{15/2}$. The purple lines show the hot bands arising from transition from the first excited state of $^4F_{9/2}$ levels¹.

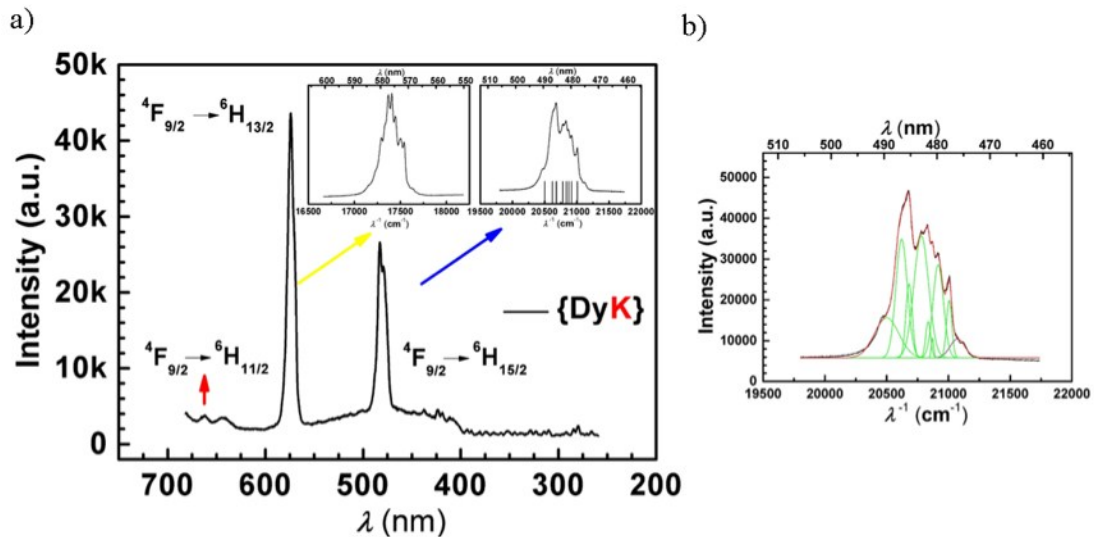


Fig. S35 (a) The emission spectrum at 77 K for $\{\text{DyK}\}$ (2) in the range of 240–690 nm and the fine spectra of transitions from $^4F_{9/2}$ to $^6H_{13/2}$ and $^6H_{15/2}$ (insets) within the duration time of 5, 10 and 20 ms respectively. (b) The Gaussian fitting for the spectrum of transition from $^4F_{9/2}$ to $^6H_{15/2}$. The purple line shows the hot bands arising from transition from the first excited state of $^4F_{9/2}$ levels.

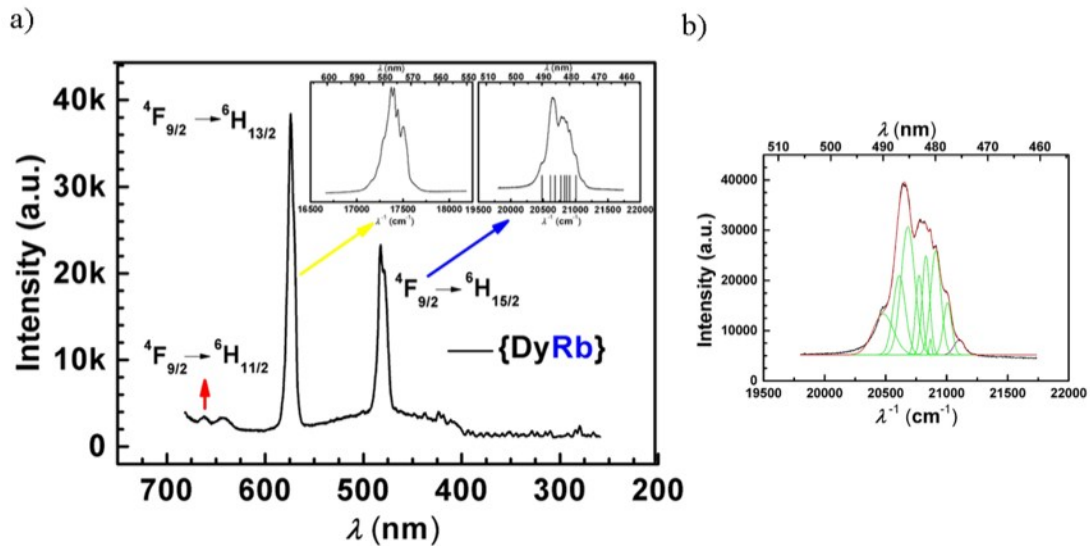


Fig. S36 The emission spectrum at 77 K for $\{\text{DyRb}\}$ (3) in the range of 240–690 nm and the fine spectra of transitions from ${}^4\text{F}_{9/2}$ to ${}^6\text{H}_{13/2}$ and ${}^6\text{H}_{15/2}$ (insets) within the duration time of 5, 10 and 20 ms respectively. (b) The Gaussian fitting for the spectrum of transition from ${}^4\text{F}_{9/2}$ to ${}^6\text{H}_{15/2}$. The purple line shows the hot bands arising from transition from the first excited state of ${}^4\text{F}_{9/2}$ levels.

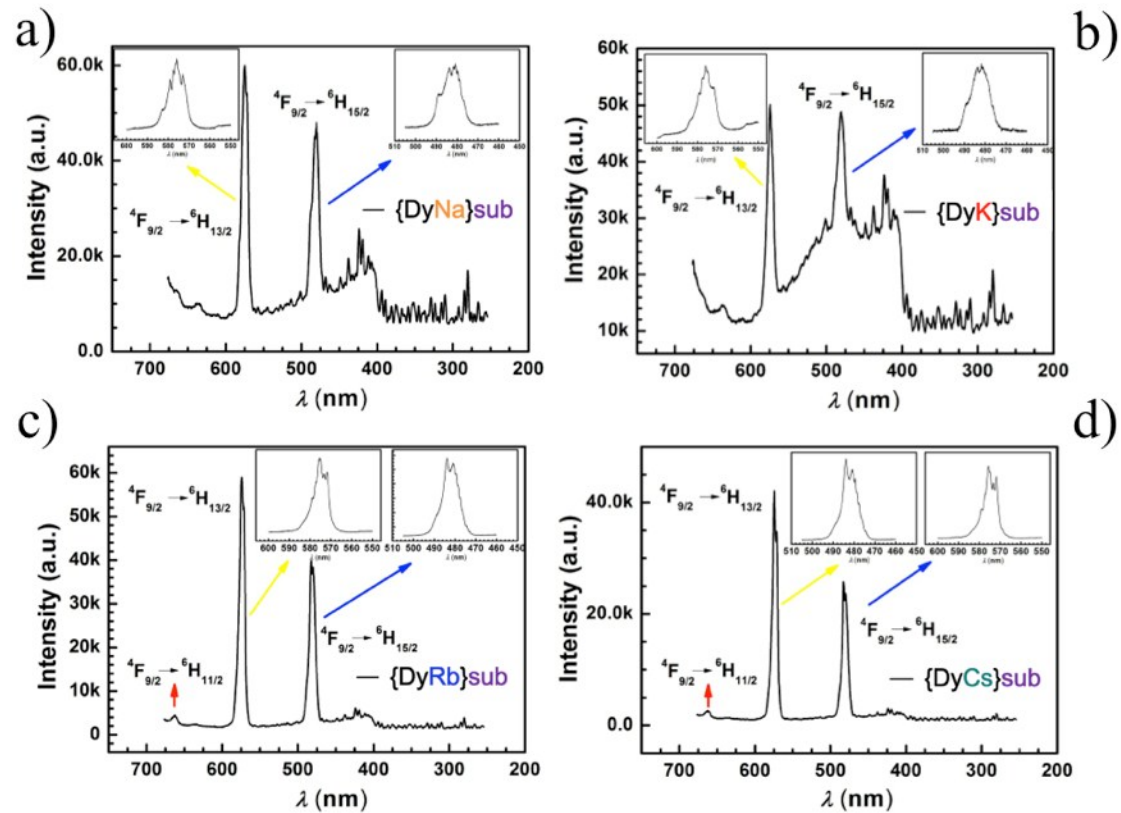


Fig. S37 (a)–(d) The emission spectra at 77 K for $\{\text{DyNa}\}_{\text{sub}}$ (5), $\{\text{DyK}\}_{\text{sub}}$ (6), $\{\text{DyRb}\}_{\text{sub}}$ (7), and $\{\text{DyCs}\}_{\text{sub}}$ (8), in the range of 240–690 nm and the fine spectra of transitions from ${}^4\text{F}_{9/2}$ to ${}^6\text{H}_{13/2}$ and ${}^6\text{H}_{15/2}$ (insets) within the duration time of 0.5, 2 and 2 s (a), 0.05, 1 and 1 s (b), 0.1, 1 and 1 s (c), 0.05, 1 and 1 s (d) respectively. Here, the sudden drop of the baseline in the emission spectrum is caused by the use of optical filter at 400 nm.

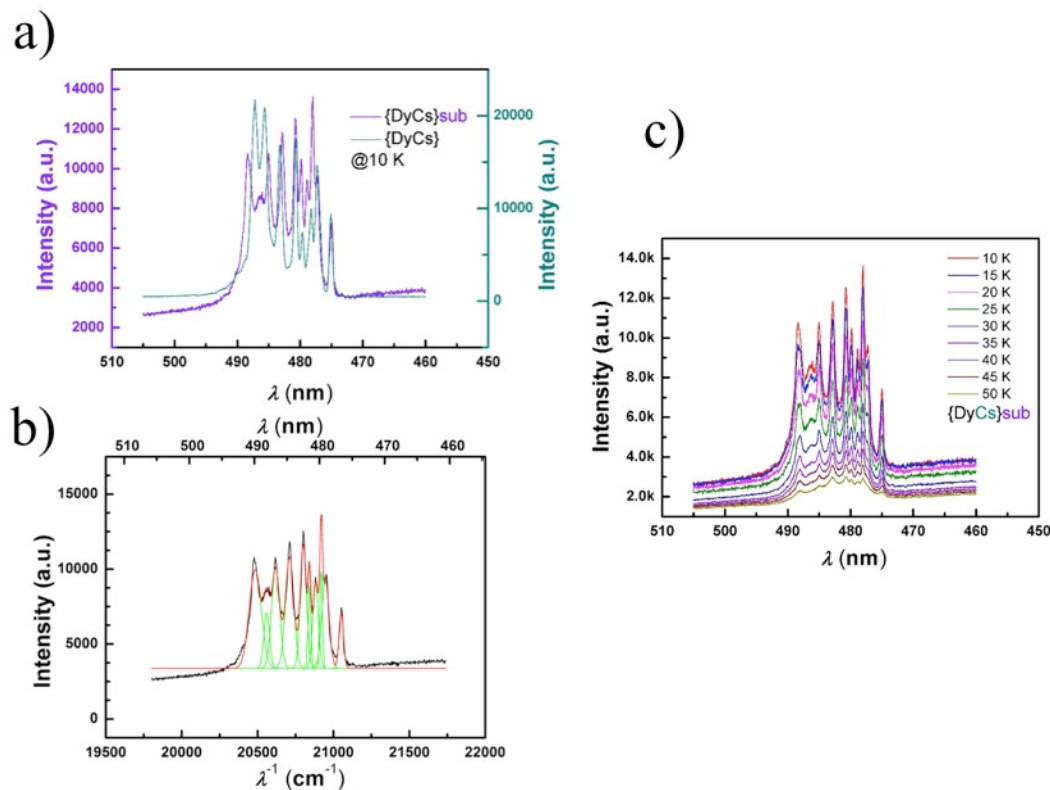


Fig. S38 (a) The fine spectrum at 10 K of the transition of ${}^4F_{9/2} \rightarrow {}^6H_{15/2}$ for Dy ion in compound $\{\text{DyCs}\}_{\text{sub}}$ (8) is compared with the one of $\{\text{DyCs}\}$ (4). (b) Fitting by Gaussian function. (c) The spectra at 10–50 K are recorded within the duration time of 100 ms for 10–25 K, 500 ms for 35–50 K. The emission intensities at different temperature are scaled to 100 ms and compared.

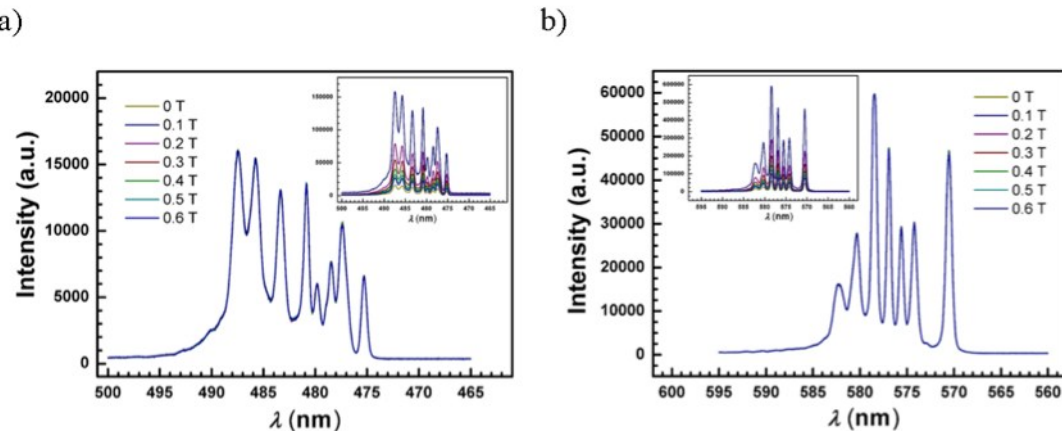


Fig. S39 (a) The emission spectrum of transition from ${}^4F_{9/2}$ to ${}^6H_{15/2}$ within 1 ms under the weak pulse magnetic field for compound $\{\text{DyCs}\}$ (4). (b) The emission spectrum of transition from ${}^4F_{9/2}$ to ${}^6H_{13/2}$ within 1 ms under the weak pulse magnetic field for compound $\{\text{DyCs}\}$. The insets in (a) and (b) show the normalized spectrum lines with the intensities divided by the corresponding value of the magnetic field.

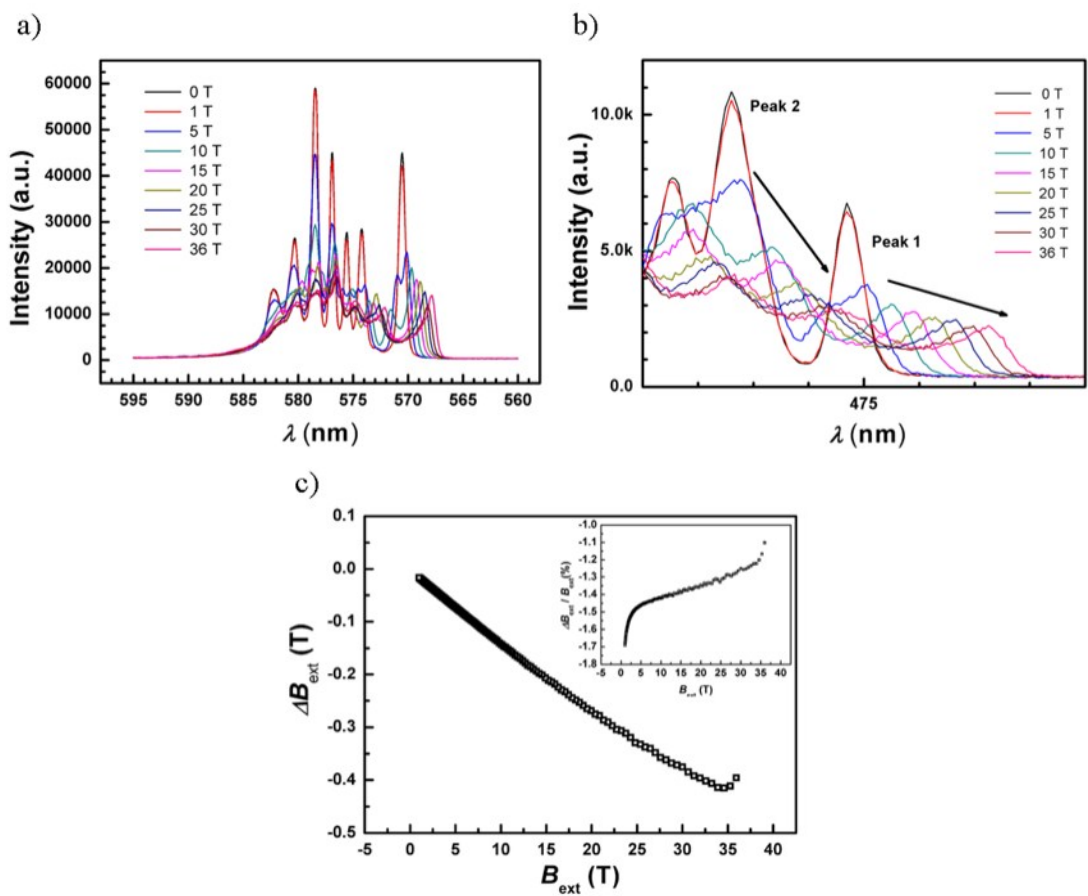


Fig. S40 (a) The luminescence spectra of the transition of ${}^4F_{9/2} \rightarrow {}^6H_{13/2}$ under the high pulse magnetic field for compound $\{\text{DyCs}\}$ (**4**). (b) The magnified spectra of the transition of ${}^4F_{9/2} \rightarrow {}^6H_{15/2}$. (c) The change of magnetic field during 1 ms under different magnetic field is less than 1.7%, and each piece of spectrum is recorded under the invariant magnetic field.

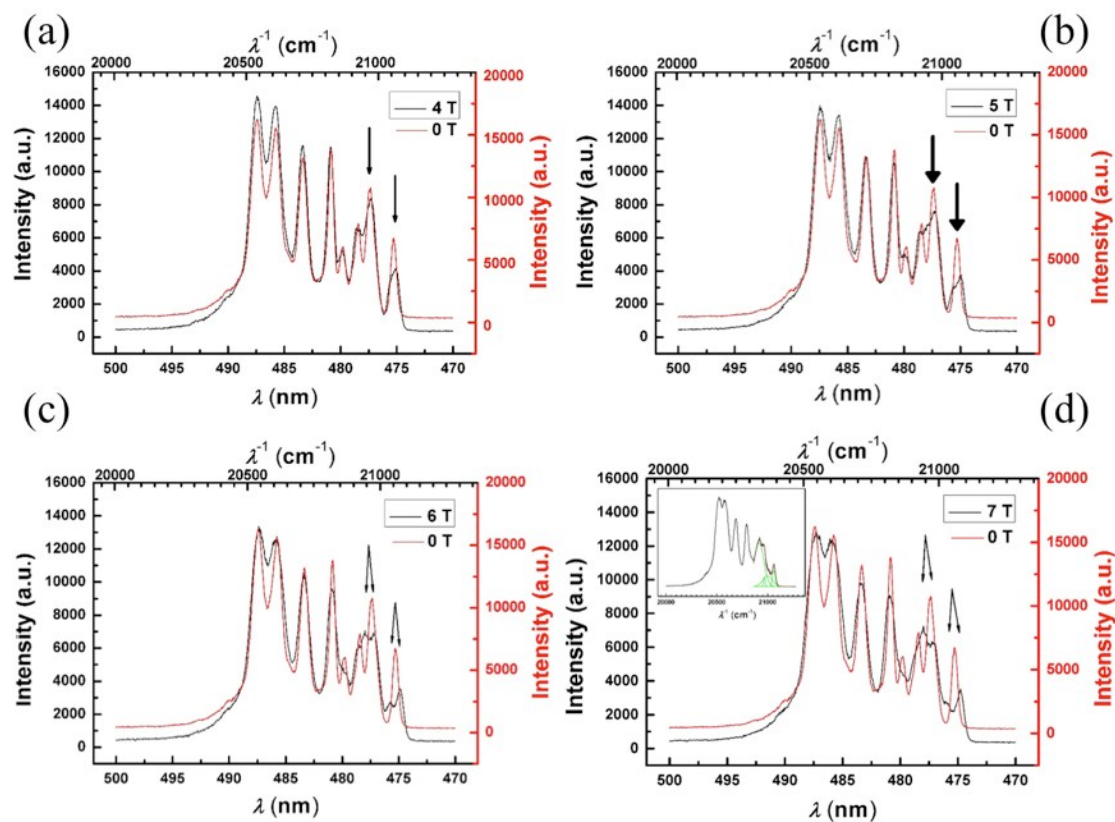
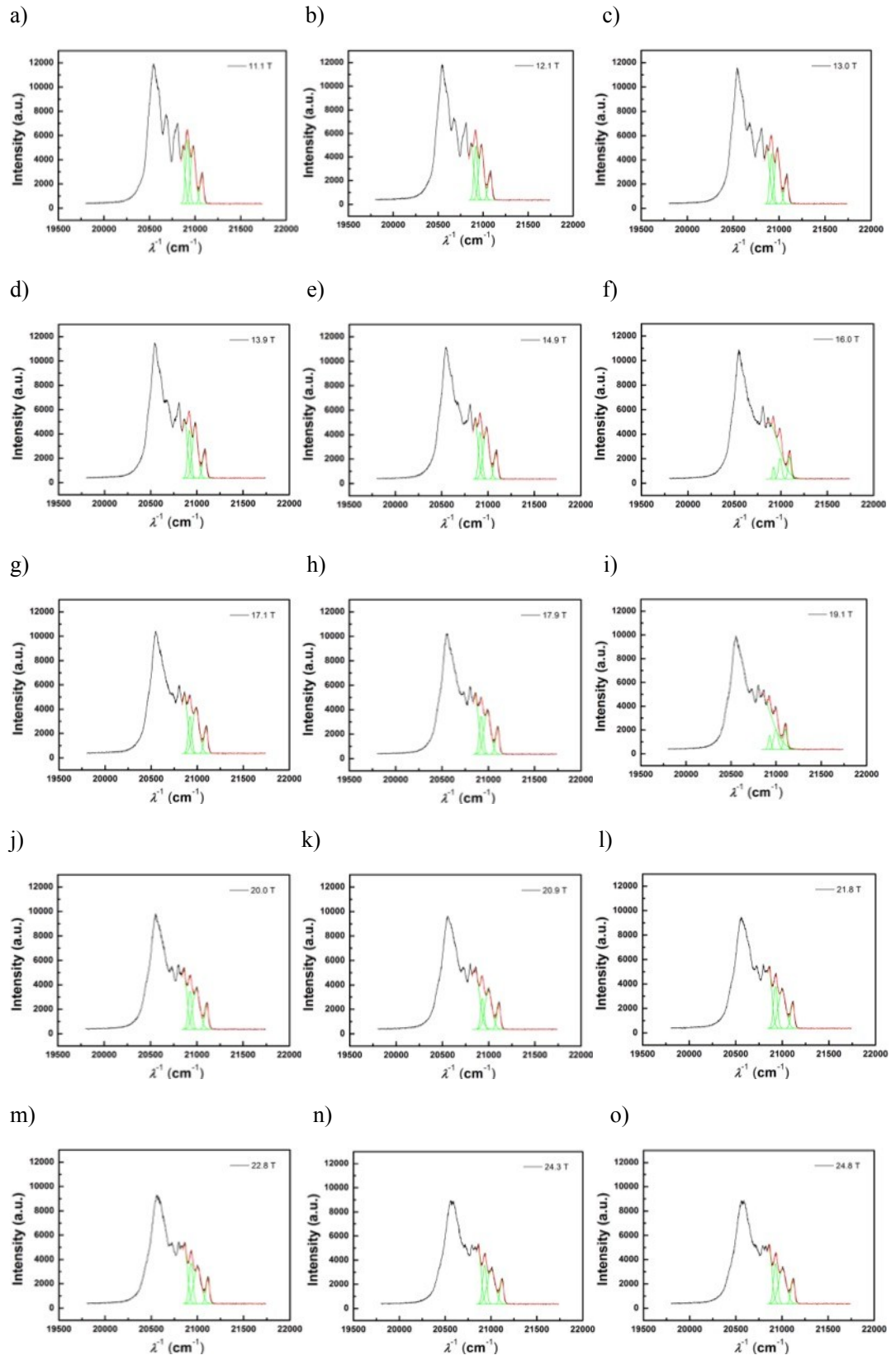


Fig. S41 (a)–(d) The emission spectra of transition from $^4\text{F}_{9/2}$ to $^6\text{H}_{15/2}$ under 4 (a), 5 (b), 6 (c), 7 (d) T for compound $\{\text{DyCs}\}$ (4). The black arrows show the splitting peaks. The Zeeman splitting energies for the ground and the excited states under 7 T are obtained by fitting the spectrum (wine line, inset).



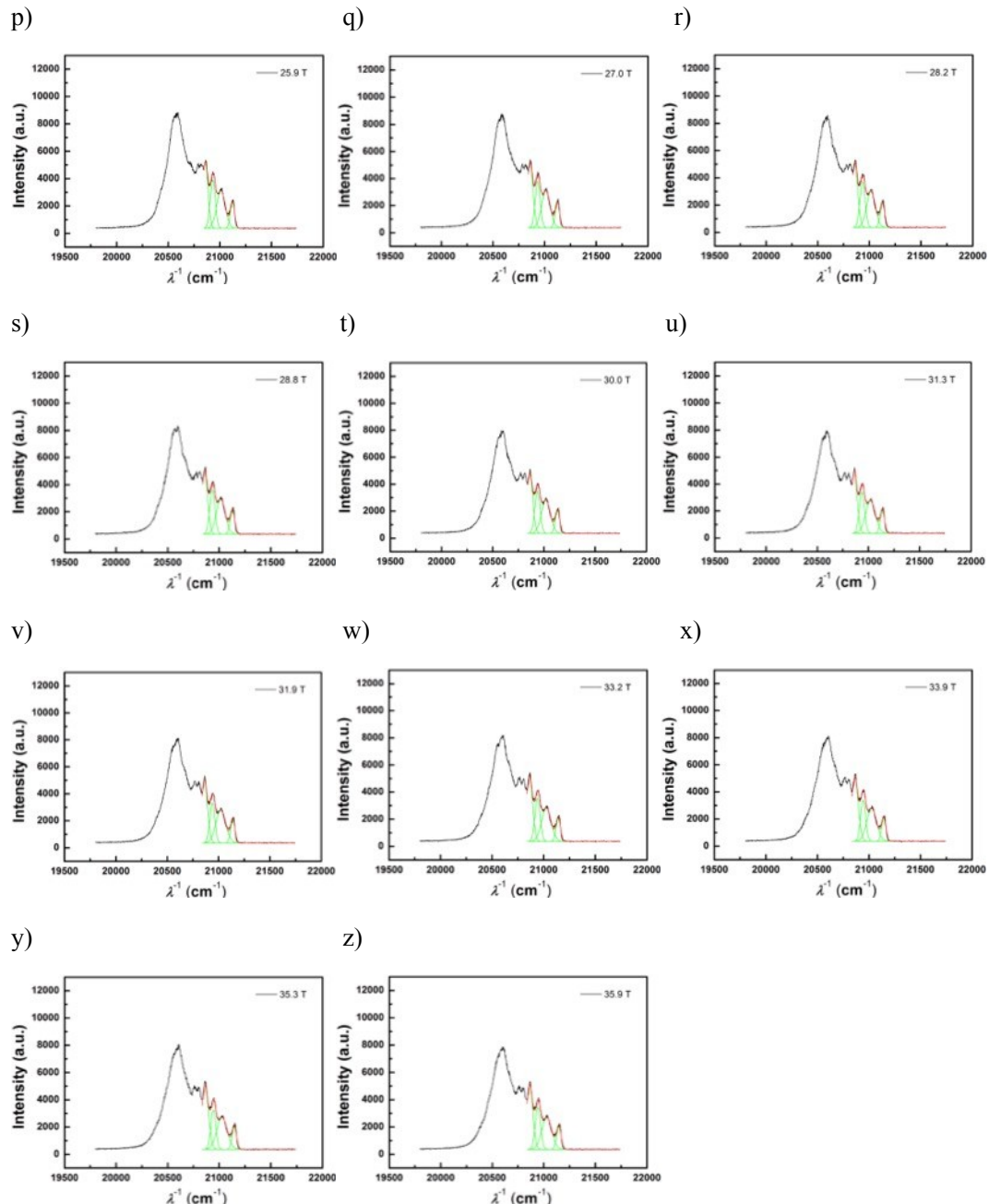


Fig. S42 (a)–(z) The parts of each emission spectra under the pulse magnetic field of 11–36 T with the step of 1 T are fitted by Gaussian function for compound {DyCs} (**4**).

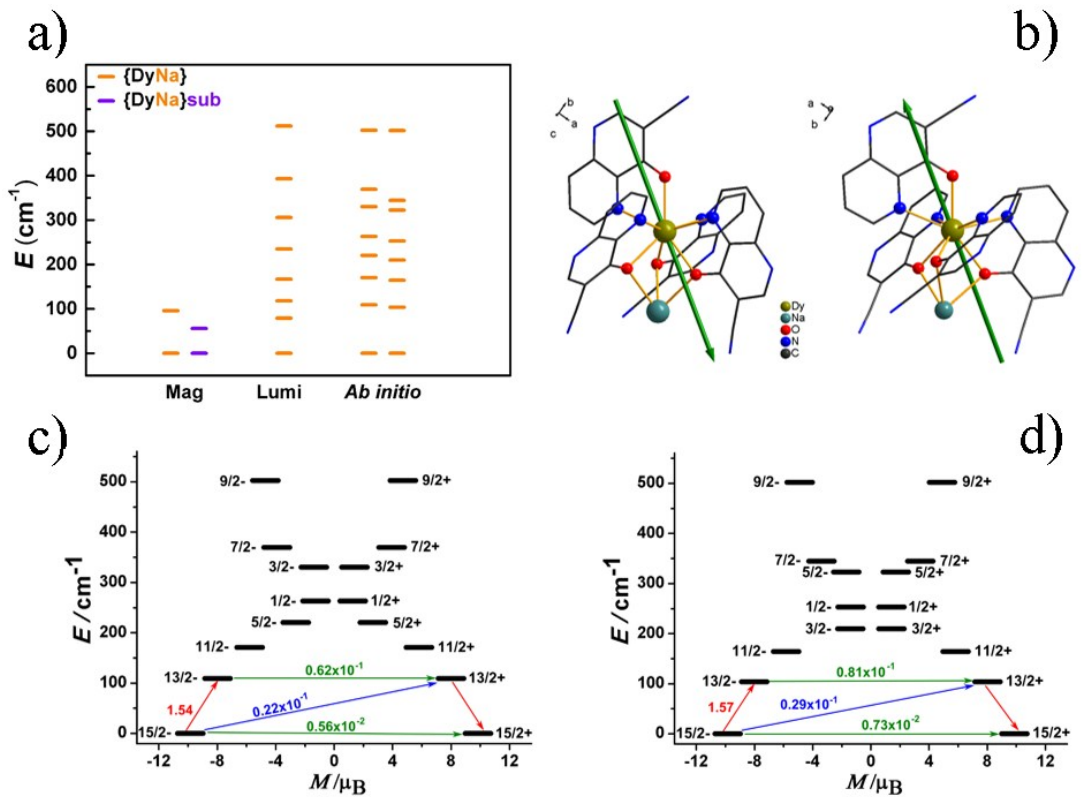


Fig. S43 (a) The energy levels for the magnetic low-lying states of the ground term by variable methods are compared for $\{\text{DyNa}\}$ (1). (b) The easy axes are depicted for Dy1 (left) and Dy2 (right) of $\{\text{DyNa}\}$. (c)–(d) The possibilities of spin reversal in different pathway are shown for Dy1 (c) and Dy2 (d) of compound $\{\text{DyNa}\}$.

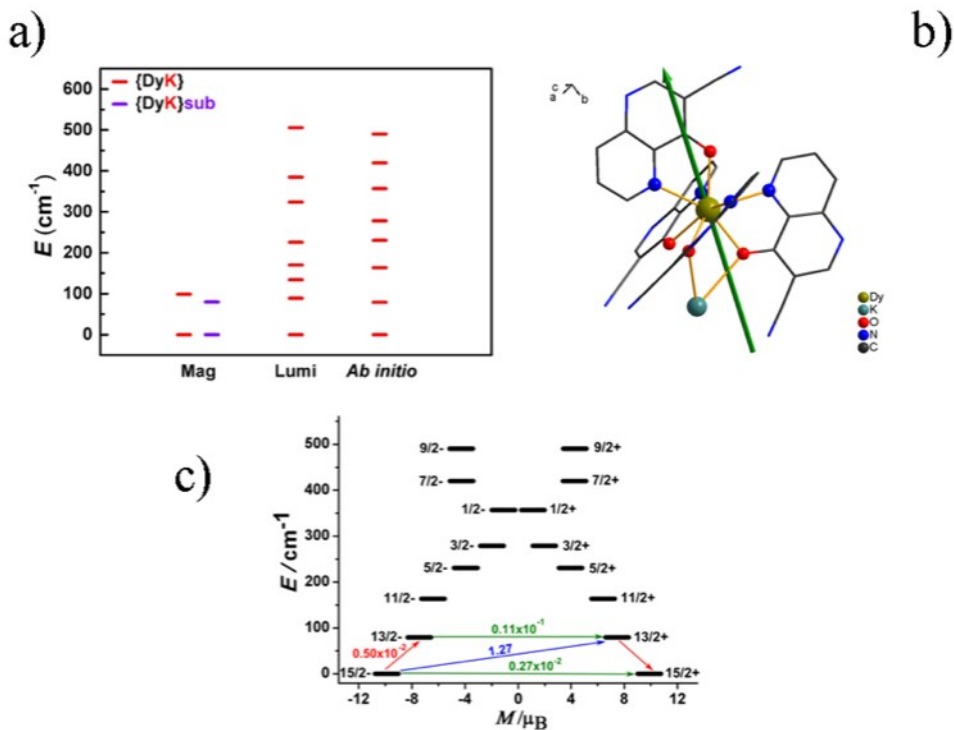


Fig. S44 (a) The energy levels for the magnetic low-lying states of the ground term by variable methods are compared for $\{\text{DyK}\}$ (2). (b) The easy axis is depicted. (c) The possibilities of spin reversal in different pathway are shown for compound $\{\text{DyK}\}$.

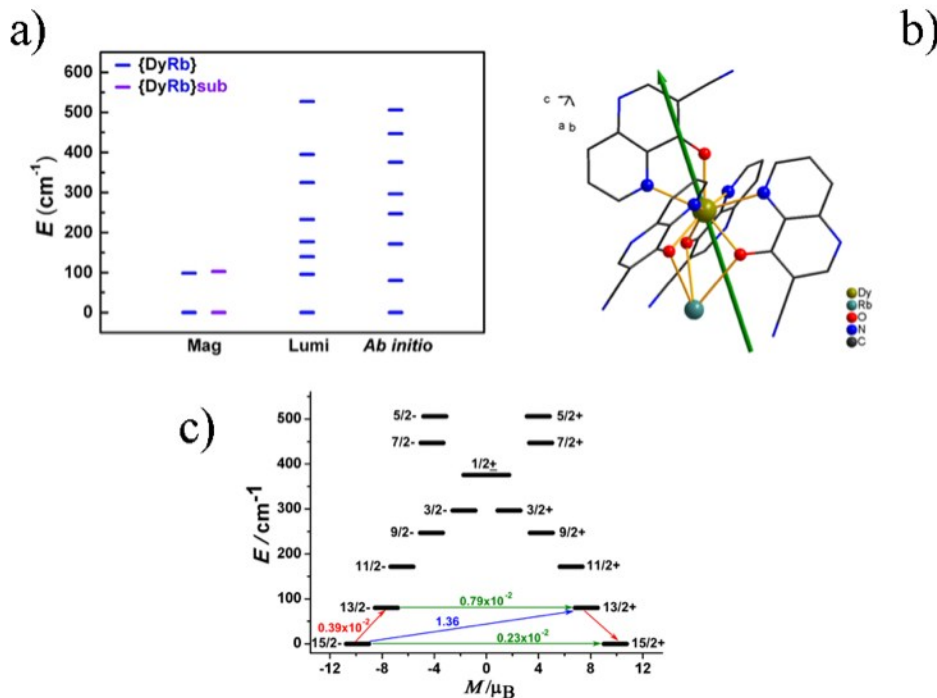


Fig. S45 (a) The energy levels for the magnetic low-lying states of the ground term by variable methods are compared for $\{\text{DyRb}\}$ (3). (b) The easy axis is depicted. (c) The possibilities of spin reversal in different pathway are shown for compound $\{\text{DyRb}\}$.

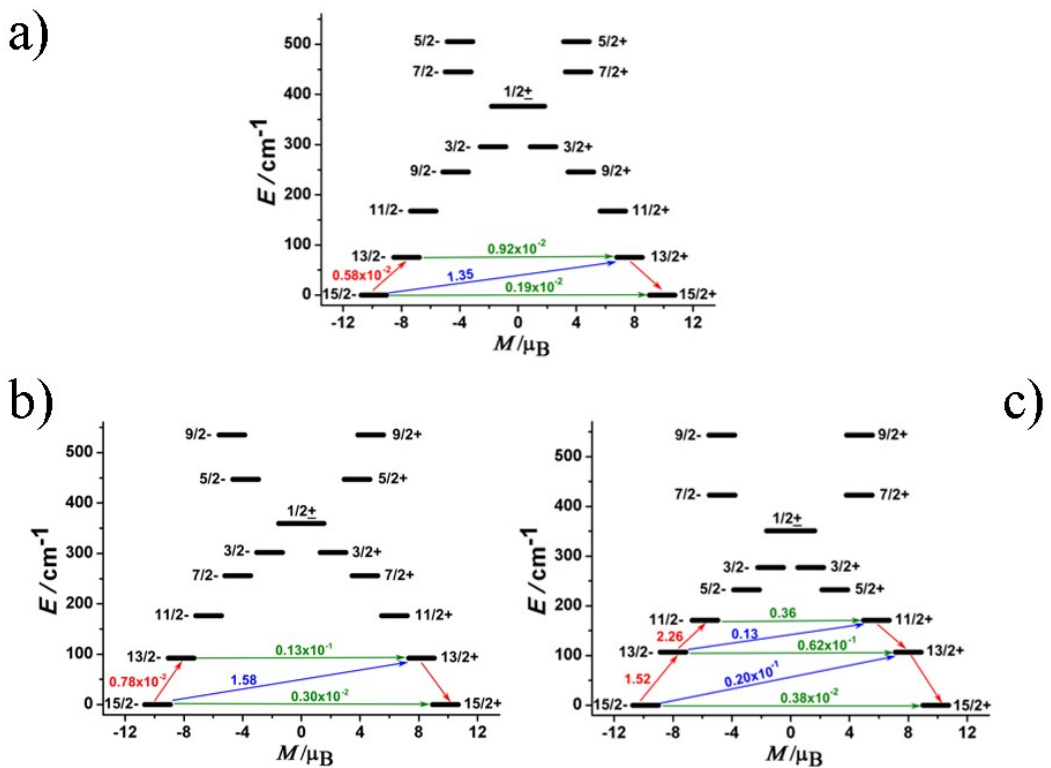


Fig. S46 (a) The possibilities of spin reversal in different pathway are shown for compound $\{\text{DyCs}\}$ (4); (b)–(c) The possibilities of spin reversal in different pathway for Dy1 (b) and Dy2 (c) of compound $\{\text{DyCs}\}_{\text{sub}}$ (8).

Table S1. Elemental analysis and MS data for the sublimed samples

	$\{\text{DyNa}\}_{\text{sub}} \textbf{(5)}$ (A = Na)	$\{\text{DyK}\}_{\text{sub}} \textbf{(6)}$ (A = K)	$\{\text{DyRb}\}_{\text{sub}} \textbf{(7)}$ (A = Rb)	$\{\text{DyCs}\}_{\text{sub}} \textbf{(8)}$ (A = Cs)
Molecular formula		$\text{C}_{40}\text{H}_{24}\text{O}_4\text{N}_{12}\text{DyA}$		$\text{C}_{160}\text{H}_{98}\text{O}_{17}\text{N}_{48}\text{Dy}_4\text{Cs}_4$
N(%)CALCD	18.23	17.91	17.07	16.21
EXP	18.09	17.93	17.09	16.21
C(%)CALCD	52.10	51.20	48.79	46.35
EXP	52.10	50.88	48.23	46.32
H(%)CALCD	2.62	2.58	2.46	2.38
EXP	2.84	2.75	2.67	2.34
[ADyL ₄ +H] ⁺ CALCD	924.13	940.11	985.05	1034.05
FOUND	924.1	940.1	985.0	1034.0
[DyL ₄] ⁻ CALCD	900.1	900.1	900.1	900.1
FOUND	900.1	900.1	900.1	900.1

Table S2. Crystallographic data and structure refinements for {DyNa}

Empirical formula	$C_{85.50}H_{61}O_{10.5}N_{24}Dy_2Na_2$ (1)	
Formula weight	1963.53	
Measurement device	SuperNova, Dual, Cu at zero, AtlasCCD	
Temperature (K)	180(2)	
Wavelength (Å)	0.71073	
Crystal system	Monoclinic	
Space group	$P2_1/n$	
	$a = 19.0396(3)$	$\alpha = 90$
Unit cell dimensions (Å , °)	$b = 20.9444(3)$	$\beta = 93.561(2)$
	$c = 20.8471(4)$	$\gamma = 90$
Volume (Å³)	8297.2 (2)	
Z	4	
Volume per non-hydrogen atom (Å³)	16.73	
Density (g cm⁻³)	1.567	
Absorption coefficient μ (mm⁻¹)	1.873	
F (000)	3896	
Theta range for data collection (°)	3.42 / 27.48	
Index ranges	$-24 \leq h \leq 24, -27 \leq k \leq 27, -27 \leq l \leq 27$	
Reflections collected	101417	
Independent reflections [$R_{\text{int}} = 0.0579$]	18992	
Completeness to theta = 27.48°	0.998	
Data/parameters/restrains	18992 / 1114 / 5	
Goodness-of-fit on F^2	1.048 / 1.046	
Final R_1 [$I > 2\sigma(I) = 13318$]	0.0677	
R_1 (all data)	0.0343	
Final wR_2 [$I > 2\sigma(I) = 13318$]	0.0839	
wR_2 (all data)	0.0692	
Largest diff. peak and hole (e Å⁻³)	1.713 / -0.739	

Table S3. Crystallographic data and structure refinements for {DyK}

Empirical formula	$\text{C}_{94}\text{H}_{80}\text{O}_{14}\text{N}_{24}\text{Dy}_2\text{K}_2$ (2)	
Formula weight	2173.02	
Measurement device	SuperNova, Dual, Cu at zero, AtlasCCD	
Temperature (K)	180(2)	
Wavelength (Å)	0.71073	
Crystal system	Triclinic	
Space group	$P \bar{1}$	
	$a = 12.3164$ (2)	$\alpha = 85.328$ (2)
Unit cell dimensions (Å , °)	$b = 14.0599$ (3)	$\beta = 68.185$ (2)
	$c = 14.9899$ (3)	$\gamma = 84.879$ (2)
Volume (Å³)	2396.98 (8)	
Z	1	
Volume per non-hydrogen atom (Å³)	17.62	
Density (g cm⁻³)	1.505	
Absorption coefficient $\mu(\text{mm}^{-1})$	1.709	
$F(000)$	1094	
Theta range for data collection (°)	3.51 / 27.48	
Index ranges	$-15 \leq h \leq 15, -18 \leq k \leq 18, -19 \leq l \leq 19$	
Reflections collected	40044	
Independent reflections [$R_{\text{int}} = 0.0336$]	10959	
Completeness to theta = 27.48°	0.997	
Data/parameters/restrains	10959 / 649 / 62	
Goodness-of-fit on F^2	1.051 / 1.049	
Final $R_1[I > 2\sigma(I)] = 9777$	0.0269	
R_1 (all data)	0.0340	
Final $wR_2[I > 2\sigma(I)] = 9777$	0.0575	
wR_2 (all data)	0.0609	
Largest diff. peak and hole (e Å⁻³)	1.299 / -0.755	

Table S4. Crystallographic data and structure refinements for {DyRb}

Empirical formula	$C_{94}H_{80}O_{14}N_{24}Dy_2Rb_2$ (3)	
Formula weight	2265.73	
Measurement device	SuperNova, Dual, Cu at zero, AtlasCCD	
Temperature (K)	180(2)	
Wavelength (Å)	0.71073	
Crystal system	Triclinic	
Space group	$P\bar{1}$	
	$a = 12.1604$ (4)	$\alpha = 83.549$ (3)
Unit cell dimensions (Å , °)	$b = 14.3443$ (5)	$\beta = 68.800$ (3)
	$c = 14.9780$ (4)	$\gamma = 83.086$ (3)
Volume (Å³)	2411.43 (13)	
Z	1	
Volume per non-hydrogen atom (Å³)	17.73	
Density (g cm⁻³)	1.560	
Absorption coefficient μ (mm⁻¹)	2.615	
F (000)	1130	
Theta range for data collection (°)	3.50 / 26.02	
Index ranges	$-14 \leq h \leq 14, -17 \leq k \leq 17, -18 \leq l \leq 18$	
Reflections collected	22324	
Independent reflections [$R_{int} = 0.0425$]	9266	
Completeness to theta = 26.02°	0.977	
Data/parameters/restrains	9266 / 609 / 14	
Goodness-of-fit on F^2	1.055 / 1.042	
Final R_1 [$I > 2\sigma(I) = 8046$]	0.0388	
R_1 (all data)	0.0483	
Final wR_2 [$I > 2\sigma(I) = 8046$]	0.0933	
wR_2 (all data)	0.1016	
Largest diff. peak and hole (e Å⁻³)	1.744 / -1.443	

Table S5. Crystallographic data and structure refinements for {DyCs}

Empirical formula	$C_{94}H_{80}O_{14}N_{24}Dy_2Cs_2$ (4)	
Formula weight	2360.61	
Measurement device	SuperNova, Dual, Cu at zero, AtlasCCD	
Temperature (K)	180(2)	
Wavelength (Å)	0.71073	
Crystal system	Triclinic	
Space group	$P\bar{1}$	
	$a = 12.1005$ (5)	$\alpha = 82.535$ (4)
Unit cell dimensions (Å , °)	$b = 14.5976$ (6)	$\beta = 69.080$ (4)
	$c = 14.9807$ (6)	$\gamma = 81.967$ (3)
Volume (Å ³)	2438.30 (17)	
Z	1	
Volume per non-hydrogen atom (Å ³)	17.93	
Density (g cm ⁻³)	1.608	
Absorption coefficient μ (mm ⁻¹)	2.330	
F (000)	1166	
Theta range for data collection (°)	3.41 / 27.48	
Index ranges	$-15 \leq h \leq 15, -18 \leq k \leq 18, -19 \leq l \leq 19$	
Reflections collected	28101	
Independent reflections [$R_{int} = 0.0402$]	10779	
Completeness to theta = 27.48°	0.964	
Data/parameters/restrains	10779 / 608 / 14	
Goodness-of-fit on F^2	0.999 / 0.994	
Final R_1 [I > 2sigma(I) = 8791]	0.0350	
R_1 (all data)	0.0509	
Final wR_2 [I > 2sigma(I) = 8791]	0.0817	
wR_2 (all data)	0.0945	
Largest diff. peak and hole (e Å ⁻³)	2.550 / -0.811	

Table S6. Crystallographic data and structure refinements for $\{\text{DyCs}\}_{\text{sub}}$

Empirical formula	$\text{C}_{160}\text{H}_{98}\text{O}_{17}\text{N}_{48}\text{Dy}_4\text{Cs}_4$ (8)	
Formula weight	4146.5	
Measurement device	SuperNova, Dual, Cu at zero, AtlasCCD	
Temperature (K)	180(2)	
Wavelength (Å)	1.54178	
Crystal system	Monoclinic	
Space group	$P2_1/n$	
	$a = 19.5421(4)$	$\alpha = 90$
Unit cell dimensions (Å , °)	$b = 19.8322(4)$	$\beta = 97.266 (2)$
	$c = 20.8863(4)$	$\gamma = 90$
Volume (Å³)	8029.7(3)	
Z	2	
Volume per non-hydrogen atom (Å³)	17.23	
Density (g cm⁻³)	1.715	
Absorption coefficient $\mu(\text{mm}^{-1})$	17.403	
$F(000)$	4028	
Theta range for data collection (°)	2.92 / 73.94	
Index ranges	$-16 \leq h \leq 24, -24 \leq k \leq 23, -25 \leq l \leq 23$	
Reflections collected	34525	
Independent reflections [$R_{\text{int}} = 0.0436$]	15847	
Completeness to theta = 73.94°	0.973	
Data/parameters/restrains	15847 / 1055 / 3	
Goodness-of-fit on F^2	1.016	
Final $R_1[I > 2\sigma(I)] = 12812$	0.0426	
R_1 (all data)	0.0554	
Final $wR_2[I > 2\sigma(I)] = 12812$	0.1084	
wR_2 (all data)	0.1177	
Largest diff. peak and hole (e Å⁻³)	1.175 / -0.867	

Table S7 The coordination bond length of Dy–O and Dy–N for compounds **1–4** and **8**

{DyNa} (1)		{DyK} (2)		{DyRb} (3)		{DyCs} (4)		{DyCs} _{sub} (8)	
Dy1–O1	2.340(2)	Dy1–O1	2.3423(16)	Dy1–O1	2.343(3)	Dy1–O1	2.341(3)	Dy1–O1	2.313(3)
Dy1–O2	2.305(2)	Dy1–O2	2.2902(17)	Dy1–O2	2.295(3)	Dy1–O2	2.297(3)	Dy1–O2	2.306(3)
Dy1–O3	2.346(2)	Dy1–O3	2.3472(17)	Dy1–O3	2.337(3)	Dy1–O3	2.335(3)	Dy1–O3	2.339(3)
Dy1–O4	2.310(2)	Dy1–O4	2.2956(17)	Dy1–O4	2.295(3)	Dy1–O4	2.295(3)	Dy1–O4	2.287(3)
Dy1–N1	2.527(3)	Dy1–N1	2.524(2)	Dy1–N1	2.514(3)	Dy1–N1	2.523(3)	Dy1–N1	2.543(4)
Dy1–N4	2.541(3)	Dy1–N4	2.581(2)	Dy1–N4	2.580(4)	Dy1–N4	2.591(3)	Dy1–N4	2.562(5)
Dy1–N7	2.479(3)	Dy1–N7	2.503(2)	Dy1–N7	2.531(3)	Dy1–N7	2.538(3)	Dy1–N7	2.513(5)
Dy1–N10	2.493(3)	Dy1–N10	2.521(2)	Dy1–N10	2.522(4)	Dy1–N10	2.522(3)	Dy1–N10	2.531(5)
*Dy1–O	2.325	*Dy1–O	2.319	*Dy1–O	2.318	*Dy1–O	2.317	*Dy1–O	2.311
*Dy1–N	2.502	*Dy1–N	2.532	*Dy1–N	2.537	*Dy1–N	2.544	*Dy1–N	2.537
Dy2–O5	2.348(2)							Dy2–O5	2.293(3)
Dy2–O6	2.306(2)							Dy2–O6	2.315(3)
Dy2–O7	2.344(2)							Dy2–O7	2.313(3)
Dy2–O8	2.306(2)							Dy2–O8	2.290(3)
Dy2–N13	2.495(3)							Dy2–N13	2.576(4)
Dy2–N16	2.554(3)							Dy2–N16	2.542(4)
Dy2–N19	2.506(3)							Dy2–N19	2.531(4)
Dy2–N22	2.497(3)							Dy2–N22	2.512(4)
*Dy2–O	2.326							*Dy2–O	2.303
*Dy2–N	2.513							*Dy2–N	2.540

*average bond length

Table S8 The bond angles of Dy for **4** and **8**

{DyCs} (4)		{DyCs} _{sub} (8)			
O(4)-Dy(1)-O(2)	138.73(10)	O(4)-Dy(1)-O(2)	142.98(13)	O(8)-Dy(2)-O(6)	143.34(11)
O(4)-Dy(1)-O(3)	131.64(9)	O(4)-Dy(1)-O(3)	126.83(12)	O(8)-Dy(2)-O(7)	124.81(12)
O(2)-Dy(1)-O(3)	79.05(9)	O(2)-Dy(1)-O(3)	79.37(13)	O(7)-Dy(2)-O(6)	80.76(12)
O(4)-Dy(1)-O(1)	129.55(10)	O(4)-Dy(1)-O(1)	127.57(13)	O(8)-Dy(2)-O(5)	130.74(12)
O(2)-Dy(1)-O(1)	80.50(10)	O(2)-Dy(1)-O(1)	79.50(13)	O(5)-Dy(2)-O(6)	76.82(12)
O(3)-Dy(1)-O(1)	72.97(9)	O(1)-Dy(1)-O(3)	76.94(13)	O(7)-Dy(2)-O(6)	80.76(12)
O(4)-Dy(1)-N(10)	67.33(11)	O(4)-Dy(1)-N(10)	67.19(14)	O(8)-Dy(2)-N(22)	67.38(12)
O(2)-Dy(1)-N(10)	153.33(11)	O(2)-Dy(1)-N(10)	149.69(14)	O(6)-Dy(2)-N(22)	148.89(12)
O(3)-Dy(1)-N(10)	76.08(10)	O(3)-Dy(1)-N(10)	75.19(14)	O(7)-Dy(2)-N(22)	80.27(12)
O(1)-Dy(1)-N(10)	83.12(10)	O(1)-Dy(1)-N(10)	78.95(13)	O(5)-Dy(2)-N(22)	74.78(13)
O(4)-Dy(1)-N(1)	77.66(10)	O(4)-Dy(1)-N(1)	76.27(13)	O(8)-Dy(2)-N(13)	74.57(14)
O(2)-Dy(1)-N(1)	94.69(10)	O(2)-Dy(1)-N(1)	97.25(13)	O(6)-Dy(2)-N(13)	103.65(13)
O(3)-Dy(1)-N(1)	139.65(10)	O(3)-Dy(1)-N(1)	143.69(13)	O(7)-Dy(2)-N(13)	139.64(12)
O(1)-Dy(1)-N(1)	66.68(10)	O(1)-Dy(1)-N(1)	66.96(13)	O(5)-Dy(2)-N(13)	66.56(13)
N(10)-Dy(1)-N(1)	97.98(11)	N(10)-Dy(1)-N(1)	93.63(14)	N(22)-Dy(2)-N(13)	76.27(13)
O(4)-Dy(1)-N(7)	78.49(10)	O(4)-Dy(1)-N(7)	78.27(14)	O(8)-Dy(2)-N(19)	77.44(14)
O(2)-Dy(1)-N(7)	95.31(10)	O(2)-Dy(1)-N(7)	92.79(14)	O(6)-Dy(2)-N(19)	92.71(14)
O(3)-Dy(1)-N(7)	66.77(10)	O(3)-Dy(1)-N(7)	66.75(15)	O(7)-Dy(2)-N(19)	66.93(13)
O(1)-Dy(1)-N(7)	139.55(10)	O(1)-Dy(1)-N(7)	143.68(14)	O(5)-Dy(2)-N(19)	142.55(13)
N(10)-Dy(1)-N(7)	83.70(10)	N(7)-Dy(1)-N(10)	92.09(15)	N(22)-Dy(2)-N(19)	102.18(14)
N(1)-Dy(1)-N(7)	153.29(11)	N(7)-Dy(1)-N(1)	149.28(14)	N(19)-Dy(2)-N(13)	150.20(14)
O(4)-Dy(1)-N(4)	72.10(11)	O(4)-Dy(1)-N(4)	76.73(13)	O(8)-Dy(2)-N(16)	77.22(13)
O(2)-Dy(1)-N(4)	66.63(10)	O(2)-Dy(1)-N(4)	66.30(13)	O(6)-Dy(2)-N(16)	66.55(13)
O(3)-Dy(1)-N(4)	131.32(10)	O(3)-Dy(1)-N(4)	130.12(14)	O(7)-Dy(2)-N(16)	134.72(13)
O(1)-Dy(1)-N(4)	129.63(10)	O(1)-Dy(1)-N(4)	126.95(13)	O(5)-Dy(2)-N(16)	122.38(14)
N(10)-Dy(1)-N(4)	138.98(11)	N(10)-Dy(1)-N(4)	143.91(14)	N(22)-Dy(2)-N(16)	141.56(13)
N(1)-Dy(1)-N(4)	78.73(11)	N(1)-Dy(1)-N(4)	78.17(14)	N(16)-Dy(2)-N(13)	80.43(13)
N(7)-Dy(1)-N(4)	82.65(10)	N(7)-Dy(1)-N(4)	79.50(15)	N(19)-Dy(2)-N(16)	83.62(14)

Table S9 The summary the parameters of the dynamic magnetic relaxation

	{DyNa}	{DyK}	{DyRb}	{DyCs}	{DyNa} _{sub}	{DyK} _{sub}	{DyRb} _{sub}	{DyCs} _{sub}
U_{eff} (cm ⁻¹) 0 Oe	18	34	42	38	-	54	59	74
1000 Oe	96	99	99	93	56	80	103	112
τ_0 (10 ⁻⁷ s) 0 Oe (10 ⁻¹⁰ s) 1000 Oe	12.4 1.69	3.74 4.16	1.73 7.23	1.86 7.58	- 27.4	0.559 47.3	0.382 7.89	0.106 4.04
Cole-Cole α 0 Oe	0.05–0.15	0.07–0.16	0.05–0.16	0.06–0.19	-	0.02–0.20	0.03–0.18	0.03–0.16
1000 Oe	0.14–0.24	0.14–0.26	0.14–0.20	0.15–0.36	0.15–0.25	0.06–0.19	0.04–0.15	0.05–0.11
$\tau_{\text{tunneling}}$ (ms)	0.038	0.089	0.09	0.13	-	0.27	0.19	0.17

Table S10 Gaussian components from fitting the luminescence spectrum at 5 K for {DyCs} (4)

	Area (E+05)	Center	Width	Height (E+03)	E (cm ⁻¹)*
1	1.48	21040.1	22	5.2	0
2	37	20949.8	35	8.5	90 ± 1
3	23	20896.8	32	5.7	143
4	13.9	20843.3	244	4.6	197
5	38.9	20795.3	30	10.3	245
6	62	20688.2	53	9.4	352
7	68	20589.5	45	11.9	451
8	91	20514.5	58	12.5	526

* E represents the energy of the magnetic sublevels of ground item for $^6\text{H}_{15/2}$ with a definition to energy of the lowest doublets of 0.

Table S11 Gaussian components from fitting the luminescence spectrum at 77 K for {DyNa} (1)

	Area (E+05)	Center	Width	Height (E+03)	E (cm ⁻¹)*
1	12	21045	216	4.49	
2	6.69	20997	46	11.6	0
3	8.3	20918	45	14.7	79 ± 3
4	7.8	20879	66	9.5	118
5	18.7	20830	70	21.3	167
6	12.83	20762	46	22.3	235
7	19.88	20691	60	26.4	306
8	32.5	20604	90	28.8	393
9	21	20485	101	16.6	512
10	12	20427	214	4.6	

* E represents the energy of the magnetic sublevels of ground item for $^6\text{H}_{15/2}$ with a definition to energy of the

lowest doublets of 0.

Table S12 Gaussian components from fitting the luminescence spectrum at 77 K for {DyK} (2)

	Area (E+05)	Center	Width	Height (E+03)	E (cm ⁻¹) [*]
1	6.9	21073	119	4.6	
2	7.6	21006	43	14.0	0
3	24.4	20917	85	22.8	89 ± 3
4	1.2	20872	20	4.8	134
5	4.4	20836	39	8.9	170
6	44.6	20780	119	29.9	226
7	11.6	20682	51	18.1	324
8	33.7	20621	93	29.1	385
9	24.2	20500	197	9.81	506

^{*} E represents the energy of the magnetic sublevels of ground item for $^6\text{H}_{15/2}$ with a definition to energy of the lowest doublets of 0.

Table S13 Gaussian components from fitting the luminescence spectrum at 77 K for {DyRb} (3)

	Area (E+05)	Center	Width	Height (E+03)	E (cm ⁻¹) [*]
1	3.2	21102	87	2.9	
2	8.9	21007	68	10.4	0
3	21.9	20911	84	20.7	96 ± 6
4	0.8	20867	19	3.2	140
5	15.3	20830	62	19.7	177
6	11.3	20774	57	15.9	233
7	36	20682	112	25.5	325
8	19.8	20612	100	15.7	395
9	17.2	20480	168	8.15	527

^{*} E represents the energy of the magnetic sublevels of ground item for $^6\text{H}_{15/2}$ with a definition to energy of the lowest doublets of 0.

Table S14 Gaussian components from fitting the photoluminescence spectrum at 10 K for {DyCs}_{sub} (8)

	Area (E+05)	Center	Width	Height (E+03)	E (cm ⁻¹) [*]
1	1.34	21051	29	3.7	0
2	3.5	20947	48	5.9	104 ± 3
3	1.4	20918.1	17	6.5	133
4	2.6	20882	40	5.7	169
5	1.3	20841.9	18	5.5	209
6	4.2	20801.3	41	8.2	250
7	5.1	20710.9	55	7.4	340
8	4.4	20618	53	6.7	433
9	1.7	20560	37	3.7	491
10	6.5	20485	79	6.6	566

^{*} E represents the energy of the magnetic sublevels of ground item for $^6\text{H}_{15/2}$ with a definition to energy of the

lowest doublets of 0.

Table S15 The values of E and g for compounds {DyNa} (**1**), {DyK}, (**2**), and {DyRb} (**3**)

KD	{DyNa}			{DyK}		{DyRb}		
	E (cm ⁻¹)	g_x, g_y, g_z	E (cm ⁻¹)	g_x, g_y, g_z	E (cm ⁻¹)	g_x, g_y, g_z	E (cm ⁻¹)	g_x, g_y, g_z
1	0.0	0.015	0.0	0.018	0.0	0.007	0.006	0.006
		0.019		0.026		0.009		0.007
		19.703		19.714		19.775		19.781
2	109.3	0.144	103.8	0.184	79.1	0.020	0.015	0.015
		0.179		0.242		0.037		0.025
		17.579		17.539		18.480		18.274
3	170.8	1.106	164.4	1.461	163.5	0.805	0.684	0.684
		1.518		2.087		1.267		1.001
		13.597		13.440		13.924		13.958
4	220.7	4.889	209.9	5.109	230.6	3.339	2.728	2.728
		5.507		6.115		3.977		3.297
		8.431		8.326		9.077		9.429
5	263.4	2.130	252.8	1.046	278.5	3.538	3.864	3.864
		2.600		1.525		4.410		5.277
		12.419		12.793		10.623		10.179
6	330.3	0.017	322.6	0.470	357.1	0.314	0.393	0.393
		1.020		2.050		0.838		0.796
		15.896		14.643		16.534		16.602
7	369.4	0.289	344.5	0.477	419.9	0.223	0.085	0.085
		0.902		2.183		0.442		0.406
		18.485		17.206		19.027		18.977
8	502.4	0.014	501.9	0.011	490.4	0.090	0.120	0.120
		0.022		0.013		0.240		0.373
		19.770		19.754		19.418		19.290

Table S16 The values of E and g for compounds $\{\text{DyCs}\}$ (4) and $\{\text{DyCs}\}_{\text{sub}}$ (8)

KD	{DyCs}		{DyCs} _{sub}			
	E (cm ⁻¹)	g_x, g_y, g_z	E (cm ⁻¹)	g_x, g_y, g_z	E (cm ⁻¹)	g_x, g_y, g_z
1	0.0	0.005		0.008		0.011
		0.006	0.0	0.010	0.0	0.013
		19.781		19.614		19.723
2	75.4	0.018		0.029		0.139
		0.028	92.1	0.040	106.9	0.185
		18.343		17.753		17.789
3	167.7	0.630		0.610		0.835
		0.897	176.6	0.750	171.2	0.970
		13.974		14.243		13.886
4	245.6	2.515		0.949		3.869
		3.098	255.8	1.724	232.2	4.880
		9.497		10.258		9.339
5	295.9	3.914		8.941		3.058
		5.643	301.7	6.917	276.9	3.854
		10.059		4.467		12.340
6	376.7	0.362		0.733		0.224
		0.781	359.7	0.884	351.2	0.424
		16.522		17.251		17.877
7	444.8	0.096		0.081		0.046
		0.409	447.1	0.110	422.4	0.142
		18.972		19.242		19.387
8	505.1	0.122		0.027		0.001
		0.362	534.9	0.060	543.1	0.017
		19.292		19.670		19.797

Table S17 The wave functions of the ground states and first excited states of the term $^6\text{H}_{15/2}$ of $\{\text{DyCs}\}$ (4)

ground states	98.6% ±15/2> + 0.7% ±11/2> + 0.4% ±9/2> + 0.3% ±7/2>
first excited states	0.2% ±15/2> + 51.7% ±13/2> + 27.8% ±11/2> + 17.9% ±9/2> + 2.2% ±7/2> + 0.2% ±5/2>

IR data:

IR for **2** : $\nu = 3582$ (br), 3047 (w), 2986 (w), 2922 (w), 2573 (w), 2214 (m), 1712 (w), 1644 (w), 1593 (w), 1558 (m), 1509 (s), 1472 (m), 1412 (m), 1376 (m), 1365 (sh), 1299 (w), 1280 (w), 1259 (w), 1230 (w), 1201 (m), 1095 (w), 1033 (w), 987 (w), 931 (w), 866 (w), 850 (w), 822 (w), 731 (m), 714 (w), 664 (w), 632 (w), 612 (w) cm^{-1} .

IR for **3** : $\nu = 3518$ (br), 3047 (w), 2986 (w), 2921 (w), 2655 (w), 2576 (w), 2213 (m), 1751 (w), 1713 (m), 1673 (w), 1630 (w), 1559 (m), 1510 (s), 1472 (m), 1412 (m), 1377 (m), 1364 (sh), 1300 (w), 1281 (w), 1259 (w), 1230 (w), 1201 (m), 1096 (w), 1033 (w), 987 (w), 931 (w), 866 (w), 822 (w), 731 (m), 714 (w), 664 (w), 632 (w), 611 (w) cm^{-1} .

IR for **4** : $\nu = 3577$ (br), 3044 (w), 2986 (w), 2922 (w), 2213 (m), 1712 (w), 1644 (w), 1592 (w), 1558 (m), 1510 (s), 1472 (m), 1443 (w), 1412 (m), 1376 (m), 1365 (sh), 1300 (w), 1281 (w), 1259 (w), 1230 (w), 1201 (m), 1095 (w), 1033 (w), 987 (w), 931 (w), 866 (w), 822 (w), 731 (m), 714 (w), 664 (w), 633 (w), 612 (w) cm^{-1} .

IR for **5** : $\nu = 3504$ (br), 3049 (w), 2986 (w), 2924 (w), 2218 (m), 1633 (w), 1596 (w), 1558 (m), 1511 (s), 1472 (m), 1413 (m), 1376 (m), 1301 (w), 1281 (w), 1261 (w), 1231 (w), 1202 (m), 1096 (w), 1033 (w), 987 (w), 932 (w), 866 (w), 850 (w), 822 (w), 731 (m), 714 (w), 667 (w), 633 (w), 612 (w) cm^{-1} .

IR for **6** : $\nu = 3645$ (br), 3556 (br), 3056 (w), 2974 (w), 2920 (w), 2876 (w), 2652 (w), 2575 (w), 2218 (m), 1928 (w), 1867 (w), 1645 (w), 1592 (w), 1558 (m), 1510 (s), 1473 (m), 1412 (m), 1376 (m), 1366 (sh), 1300 (w), 1280 (w), 1259 (w), 1231 (w), 1201 (m), 1094 (w), 1033 (w), 985 (w), 968 (w), 961 (w), 931 (w), 865 (w), 848 (w), 822 (w), 731 (m), 714 (w) cm^{-1} .

IR for **7** : $\nu = 3554$ (br), 3046 (w), 2985 (w), 2922 (w), 2216 (m), 1644 (w), 1594 (w), 1558 (m), 1510 (s), 1473 (m), 1412 (m), 1376 (m), 1300 (w), 1280 (w), 1259 (w), 1231 (w), 1201 (m), 1095 (w), 1033 (w), 986 (w), 931 (w), 865 (w), 848 (w), 822 (w), 731 (m), 714 (w), 664 (w), 633 (w), 612 (w) cm^{-1} .

IR for **8** : $\nu = 3469$ (br), 3046 (w), 2960 (w), 2921 (w), 2839 (w), 2214 (m), 1645 (w), 1592 (w), 1558 (m), 1511 (s), 1473 (m), 1412 (m), 1376 (m), 1366 (sh), 1299 (w), 1280 (w), 1259 (w), 1231 (w), 1201 (m), 1165 (w), 1094 (w), 1033 (w), 987 (w), 968 (w), 930 (w), 865 (w), 849 (w), 822 (w), 731 (m), 714 (w), 664 (w), 633 (w), 614 (w) cm^{-1} .

Reference:

1. J. Long, R. Vallat, R. A. S. Ferreira, L. D. Carlos, F. A. Almeida Paz, Y. Guari and J. Larionova, *Chem. Commun.*, 2012, **48**, 9974-9976.